Available online at www.sciencedirect.com

ScienceDirect

journal homepage: www.elsevier.com/locate/he

Methanation of CO_2 on Cu in a tubular co-ionic SOEC

Esperanza Ruiz [a,*], *Juan Aldecoa* [b,1], *Ángel Morales* [a], *Meryem Farchado* [a], *José María Sánchez* [a]

[a] *Centro de Investigaciones Energéticas, Medioambientales y Tecnológicas (CIEMAT), Av. Complutense, 40, 28040 Madrid, Spain*

[b] *The Association of European Renewable Energy Research Centers (EUREC), Place du Champ de Mars 2, 1050, Brussels, Belgium*

HIGHLIGHTS

- CO_2 methanation on Cu/BZCY in a tubular cell configuration under realistic conditions.
- Control of CH_4 production by modifying the applied potential at medium temperatures.
- Maximum CH_4 yield and Faradaic efficiency and minimum energy cost at −0.5V and 450 °C.
- Minimum CO selectivity associated with lower CH_4 purification cost at −0.5V and 450 °C.

GRAPHICAL ABSTRACT

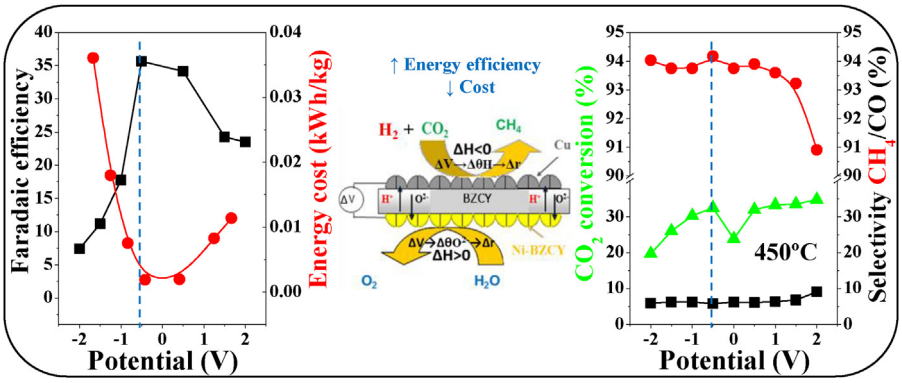

ARTICLE INFO

Article history:
Received 30 November 2022
Received in revised form
25 August 2023
Accepted 29 August 2023
Available online 15 September 2023

Keywords:
CO_2 methanation
Cu
co-ionic SOEC

ABSTRACT

This work aims contributing to develop a cathode for CO_2 methanation in tubular co-ionic (H^+/O^{2-} conducting) SOECs and to cell operation optimization to decrease energy input and costs for advancing process application. It studies the effect of temperature (325-550 °C) and potential (from −2 to +2 V at 450 °C) on CO_2 conversion and selectivity to CH_4 and CO, at bench scale, at atmospheric pressure and using high flowrates (42 NL/h) and realistic compositions ($4H_2/CO_2$ binary mix), over a Cu film (<2 μm) coated by electroless on an anode (Ni-BZCY)-supported solid electrolyte (BZCY) candle. CH_4 preferentially forms over CO. CH_4 selectivity increases with temperature up to 97.3% at 400 °C, from which, CH_4 and CO selectivity decreases and increases, respectively. The optimum potential is −0.5V, as maximizes CH_4 selectivity (94.2%) and minimizes energy cost (0.002 kWh/kg CH_4) with high

* *Corresponding author.*
E-mail address: esperanza.ruiz@ciemat.es (E. Ruiz).
[1] Present address: Sisener Ingenieros S.L., Paseo Independencia 16, 1st Floor, 50004, Zaragoza, Spain.

https://doi.org/10.1016/j.ijhydene.2023.08.325

Bench scale
PtG
H_2 carriers

CO_2 conversion (32.5%) and low CO selectivity (5.8%), resulting in higher CH_4 yield and lower CH_4 purification cost.

1. Introduction

Excessive consumption of fossil fuels during the last centuries resulted in the growing of CO_2 atmospheric concentrations, linked with detrimental global warming, and in the declining of available fossil resources. On the other hand, rapid growth of renewable energy has resulted in a demand of new efficient technologies that can handle renewable energy fluctuation and enhance its integration. Conversion of carbon dioxide to grid compatible synthetic natural gas may contribute to diminish CO_2 emissions and the reliance on fossil reserves, enabling CO_2 recycling as a renewable, safe and established fuel, as well as the storage of the surplus of renewable energy required to power the production of H_2 by water electrolysis and the chemical conversion process through the so-called Power to Gas (PtG) technology [1]. Therefore, PtG could contribute both to the integration of renewable energy and to the reduction of CO_2 emissions. This technology represents also a way for H_2 chemical storage in the form of hydrogen-rich energy carriers such as CH_4, as H_2 can also be afterwards extracted from synthetic natural gas, even with no need for external energy, by auto-thermal steam reforming [2]. In fact, the European Union has contemplated the contribution of hydrogen and power to gas technologies in the long-term strategy to achieve climate neutrality in 2050 [3].

Electrolysis of H_2O and CO_2 is considered to be a promising approach for renewable energy storage via sustainable production of H_2 and hydrocarbon fuels [4]. CH_4 can also be synthesized in situ in solid oxide electrolysis cells (SOECs) powered by renewable energy, which potentially enables combining H_2 production by water electrolysis and CO_2 hydrogenation in a single unit making renewable energy storage possible. In addition, given that electrolysis is an endothermic reaction whereas methanation is a highly exothermic one, the coupling of both reaction in SOECs can result in an enhanced overall energy efficiency of the system [4], but this integration is not straightforward given the dissimilar operating temperatures required for conventional oxygen ion conducting SOECs (600-1000 °C) and methanation reaction (<400 °C), which resulted in methane yields below 1% [5–7] on Ni or GDC based cermet cathodes in single temperature zone cell configuration at atmospheric pressure. In addition, the presence of water co-fed with CO_2 or produced by CO_2 methanation shifts the reaction equilibrium to the reactants side. Different approaches have been utilized to improve CH_4 yield such as co-feeding H_2 with CO_2 and H_2O to the SOEC cathode, decreasing operation temperature [8], introducing a methanation catalyst, placed over [9], next to [10,11] or infiltrated [7,12] in the SOEC cathode, increasing the operating pressure [13–15] or/and using a dual temperature zone SOEC configurations [9–11,14] where the low temperature zone favours the methanation of the syngas generated by H_2O and CO_2 co-electrolysis in the high temperature region. All of these innovations [8–16] enabled to reach CH_4 yields up to about 29%. Lately, lo Faro et al. reported a methane yield of 67% at 525 °C on a Ni–Fe based catalyst coated conventional SOEC cathode [16]. More recently, Baxter et al. reported to achieve CO_2 conversion and CH_4 selectivity values close to 100% at 450 °C on a commercial Ni based methanation catalyst coated standard SOEC cathode [17]. One of the main conclusion of these studies was that the use of an intermediate temperature ion conducting electrolyte could be more appropriate for in situ methane synthesis in SOECs [4,16,17]. In this way, proton conducting SOECs are able to operate at temperatures between 400 and 600 °C. In addition, protonic SOECs enable separate feeding of CO_2 and H_2O at opposite electrodes, i.e. water electrolysis and CO_2 methanation takes place at the anode and cathode chamber of the SOEC, respectively, resulting in higher methanation conversion as equilibrium is not limited by the co-feeding of water. Moreover, in this case CH_4 yield can be improved by co-feeding the cathode with the surplus of hydrogen recycled from the anode, with no need for an external source of hydrogen [18]. Xie et al. [19] obtained CH_4 yields up to 2.4% over a composite BCZYZ and Fe electrocatalyst in a proton conducting SOEC operating at 614 °C. Li et al. [20] achieved CH_4 selectivities in the range of 92–96% on an Ir–CeO_2 based cathode in a similar protonic SOEC operating at 400 °C. Duan et al. [21] produced methane with about 40% of methane yield at around 300 °C on a Ni–CeO_2 based cathodic catalyst in a protonic SOEC.

Moreover, it has been reported [4,18] that the electrocatalytic synthesis of methane from CO_2 in both oxygen or proton conducting SOECs exhibits an EPOC (Electrochemical Promotion of Catalysis) effect which gives rise to higher methane yield than conventional thermocatalytic CO_2 methanation due to the promoting effect of oxygen ion or proton pumping to or from the catalyst electrode surface, as will be explained in more detail later.

Therefore, in situ methanation in SOECs is still at an early stage of development and needs substantial research to develop cathode electrocatalysts active for the methanation reaction and to optimize reactor design and cell operating conditions, such as temperature and applied potential [17]. The potential practical application of in situ CO_2 methanation in SOECs would require [22–30]: (a) decrease the operating temperature of the system, via increasing the activity and selectivity of the catalysts and the ionic conductivity of solid electrolytes, with consequent increase in energy efficiency and in the stability and durability of electrocatalyst and solid electrolytes (in the presence of CO_2, H_2O, etc.), by using O^{2-} and H^+ co-conducting intermediate temperature solid oxide electrolytes, by decreasing particle size and increasing dispersion of catalyst or by addition of promoters or co-

catalysts; (b) decrease the cost of the system using catalysts based on cheaper and more easily available metals; (c) reduce the ohmic losses by decreasing electrode thickness, by increasing ionic conductivity of electrolytes and electronic conductivity of electrodes and by the use of electrode supported thin electrolyte systems; (d) increase the simplicity and scalability of the systems, for example by developing easily scalable procedures allowing to prepare porous electrocatalyst thin films and proper reaction configurations (tubular, monolithic, etc.) and (e) their study under realistic conditions, representative of potential practical application at a proper scale, for evaluation of their technical feasibility. In addition, the key challenges for advancing CO_2 conversion to fuels are increasing the energy efficiency, decreasing the capital (CAPEX) and operating (OPEX) costs of the process and integration of renewable energy sources [26,31]. To fulfil these challenges high energy efficiency, reaction rates and long-term stability are required. High energy efficiency is achieved through high activity and selectivity (high faradaic efficiency in product formation) at low operation temperature and low overpotentials to maximize product yield with a minimum energy cost. High selectivity can result also in lower product separation costs. On the other hand, the reaction rate determines the reactor size and the CAPEX of the process, i.e., high reaction rate can result in a decrease of size and cost of the SOEC system [26,30]. High long-term stability of the catalyst is also crucial to reduce the OPEX associated with regeneration or replacement of the spent catalyst [30].

Electrochemically assisted catalytic CO_2 hydrogenation is regarded as a ground-breaking technology to achieve these challenges. In fact, the application of small potentials or currents between a metal catalyst deposited on a solid electrolyte and a counter electrode results in the moving of ionic promoting species, to or from the catalyst surface, enabling in-situ modification of the relative chemisorption between the different coexistent reaction gases (e.g. CO_2, H_2), which allows enhancing the catalytic activity for the CO_2 hydrogenation reaction, altering the selectivity to the preferred product (CH_4) and electrochemically monitoring the process [32]. Moreover, in double chamber reactor configuration (SOEC), the protons produced via H_2O electrolysis (or other H^+ producing reaction) over the anode are transferred through the solid electrolyte membrane to the cathode, where CH_4 can be formed by reaction with CO_2, which may enable also combining H_2 production by H_2O electrolysis (endothermic) and CO_2 hydrogenation (exothermic) in the same reactor, making renewable energy storage possible [33] and resulting in a more compact and smaller system, with adequate thermal control of the whole (with the consequent energy savings, and reduced investment and operating costs) [34]. The latter represent a considerable advantage over conventional fixed-bed reactors, since the methanation reaction is very exothermic and can lead to a temperature increase in the catalytic bed which limits equilibrium conversion and can cause hydrothermal deactivation of the catalyst [35,36], making necessary the use intermediate cooling steps or gas recycling to control catalyst overheating at the expense of complicating the design and increasing the size of the methanation reactor. The double chamber reactor configuration (SOEC) is based on the use of solid electrolytes with appropriate protonic (H^+) or co-ionic (H^+ and O^{2-}) and even electronic (e^-) conductivity at the temperature required for the application of the specific system [28,37], such as co-ionic O^{2-} and H^+ co-conducting intermediate temperature solid oxide electrolytes.

It has been confirmed [28,37] that electrochemically enhanced catalytic CO_2 hydrogenation has some advantages over conventional catalytic technologies, given that it may allow: (a) shifting the equilibrium of the CO_2 hydrogenation reaction (e.g. by electrochemical pumping of highly active H^+ species to the catalyst surface) avoiding the use of high pressures and increasing the reaction rate (e.g. by O^{2-} removal from the catalyst surface enhancing CO_2 activation and accelerating the CO_2 hydrogenation reaction), and, therefore, the operation of the catalyst under milder pressure (atmospheric) and/or temperature conditions with lower residence times and higher conversion per pass, resulting in a decrease in reactor size (decreasing CAPEX), energy costs (e.g. preheating, pumping, compression) and OPEX; (b) altering the selectivity to the desired product (e.g. CH_4) by electrochemically adjusting H_2/CO_2 surface coverage ratio to that stoichiometrically required for the synthesis reaction (e.g. $H_2/CO_2 = 4$ for the methanation reaction), with subsequent increase in energy efficiency in product formation and decrease in OPEX associated with product purification; (c) improving catalyst tolerance to coexistent inhibitors or poisons by electrochemically retarding their chemisorption (e.g. decreasing surface coverage of H_2O) and increasing catalyst life time by in-situ tuning of catalyst activity/selectivity, via varying applied potential instead of increasing temperature (which results in a loss of selectivity) or decreasing treatment capacity (concentrated CO_2 stream flow rate) as typical for conventional catalytic technologies, or by in-situ electrochemical regeneration, by decomposition of potentially formed surface poisonous species (e.g. carbonates) via reversal polarization and oxidation or gasification of deposited carbon by pumping of oxygen to the catalyst surface (in O^{2-} or co-ionic conducting reactors) or by increasing surface coverage of H_2O, respectively, with subsequent decrease in OPEX associated with catalyst regeneration or replacement; (d) monitoring and controlling the reaction simultaneously during the process, by measurement of the generated current variation (use as an electrochemical sensor), with no need for gas analysis, with the subsequent decrease in CAPEX and OPEX associated with process instrumentation and control.

As Table 1 shows, the electrochemically assisted catalytic CO_2 hydrogenation has been studied by other groups over Pt on YSZ (an O^{2-} conductor) [38–40], Pd on SCY (a proton conductor) [41], YSZ or Na-βAl_2O_3 (a Na^+ conductor) [42], Rh on YSZ [38,43], Ru on YSZ, Na-βAl_2O_3, K-βAl_2O_3 (a K^+ conductor) or BZY (a proton conductor) [44–53], free-standing and Co_3O_4 supported Ru nanoparticles on BZY [54], Ru nanoparticles or Ni or Ru impregnated carbon nanofibers on YSZ [55], Ni on K-βAl_2O_3 [56], Ni nanoparticles on YSZ [57], nanodispersed Ru–Co on BZY [58], Fe-oxide [59] or Ru–Fe oxide [60] nanowires on YSZ and PdZn alloys on Na-βAl_2O_3 or K-βAl_2O_3 [61]. However, the hydrogenation of CO_2 on Cu in solid electrolyte ion conducting reactors has been less explored. It has been studied over Cu on TiO_2-YSZ [38], Cu on $SrZr_{0.9}Y_{0.1}O_{3-\alpha}$ (a proton conductor) [62], and Cu nanoparticles [63] or Co_3O_4

Table 1 – Comparative of studies on electrochemically assisted catalytic hydrogenation of CO_2.

Catalyst	Electrolyte/ configuration	Coating method	Operating conditions	XCO_2 (%)	Selectivity	Rate (mol/s)	$\|\Delta\|_{max}$	Ref.
Pd	SCY (H^+) disk (double chamber)	–	450-700 °C, 1.3NL/min CO_2 (0.09–1.1%) in He (cathode)/H_2 (anode)	–	100% CO	rCO≅1 E–09 (450 °C, 1.1% CO_2)	0.3	[41]
Cu	SZY (H^+)/disk (double chamber)	–	550–750 °C, 1.2–1.8NL/h CO_2 (0.6–2.4%) in He (cathode)/H_2 (anode)	–	100% CO	rCO<1 E–09 (600 °C, 1.1% CO_2)	2	[62]
Pt	YSZ (O^{2-}) tube (Fuel cell type)	Organometallic paste	650–800 °C, 1.2NL/h, −2 to +2V CO_2 (1–10%) and H_2 (1–10%) in He		100% CO	rCO≅ 5 E–08 (725 °C, H_2/CO_2 = 4, -1V) rCO≅ 20 E–08 (650 °C, H_2/CO_2 = 1, -1V)	10	[39]
Pd	YSZ (O^{2-}) tube (Fuel cell type)	Organometallic paste	490–589 °C, 2.3–18NL/h, −1.2 to −2.2V CO_2 (19.3–21.5%) and H_2 (49 –73.3%) in N_2	–	100% CO	rCO≅ 7 E–09 (589 °C, H_2/CO_2 = 4, −2.2V, low disp. Pd, 12NL/h) rCO≅ 8 E–09 (533 °C, H_2/CO_2 = 2, −2.2V, high disp. Pd, 8NL/h)	150	[42]
	Na-ß-Al_2O_3 (Na^+) disk (Fuel cell type)		545–605 °C, 2.3–18NL/h, −1.2 to −2.2V CO_2 (19.3–21.5%) and H_2 (49 –73.3%) in N_2	–	100% CO	rCO≅ 2 E–09 (545 °C, H_2/CO_2 = 3.5, −1.2V, 4.4NL/h)	–	
Rh	YSZ (O^{2-}) tube (Fuel cell type)	Organometallic paste	328–477 °C, 0.9–3NL/h, −0.4 to −1.6V CO_2 (1–10%) and H_2 (1.5 –90%) in He	–	SCH_4≅19% (451 °C, H_2/CO_2 = 1.5, 2.3NL/h, −0.6V)	rCH_4≅ 2.9 E–09	210	[43]
Rh	YSZ (monolithic type)	Sputtering	280–380 °C, 60NL/h, −3 to +3V CO_2 (1%) and H_2 (5.6%) in He	5	SCH_4≅12% (380 °C, -3V, H_2/CO_2 = 5.6)	rCH_4≅ 0.4 E–07	–	[38]
Pt			380 °C, 60NL/h, −4 to +4V CO_2 (1%) and H_2 (5.6%) in He	2.5	100% CO (380 °C, H_2/CO_2 = 5.6, +4V)	rCO≅1.6 E–07	–	
Cu/TiO_2			220–380 °C, 60NL/h, ±3V CO_2 (1%) and H_2 (5.6%) in He	≅40	SCH_4≅35% (380 °C,-3V, H_2/CO_2 = 5.6)	rCH_4≅ 0.9 E–06	0.3	
				≅30	SCH_4≅39% (380 °C, +3V, H_2/CO_2 = 5.6)	rCH_4≅ 1.1 E–06		
			220–380 °C, 60NL/h, CO_2 (1%), H_2 (5.6%) & CH_3OH (0.5%) in He	–	SCH_4≅100% (±3V & O.C.)	–	–	
Ni-carbon nanofibers (CNF)	YSZ disk (single chamber)	Impregnation & sputtering	300–450 °C, 6NL/h, −1.5 to +1.5V CO_2 (1%) and H_2 (5.6%) in He	–	SCH_4≅15% (440 °C, −0.7V)	rCH_4≅ 4 E–08	–	[55]
Ru–CNF				–	SCH_4≅55% (440 °C, −0.24V)	rCH_4≅ 0.35 E–08	–	
Ru	YSZ disk (single chamber)	Impregnation	200–340 °C, 12NL/h, ±1V CO_2 (0.5–2%) and H_2 (0.1 –15%) in He	–	SCH_4≅14% (+1V) SCH_4≅6% (-1V) (300 °C, H_2/CO_2 = 7)	rCH_4≅ 0.5 E–07 (±1V)	1000	[44]

(continued on next page)

Table 1 – (*continued*)

Catalyst	Electrolyte/ configuration	Coating method	Operating conditions	XCO_2 (%)	Selectivity	Rate (mol/s)	$\lvert\Lambda\rvert_{max}$	Ref.
Ru	K-ß-Al_2O_3 disk (single chamber)	Impregnation	280–420 °C, 6NL/h, −0.8 to 0.8V CO_2 (0.25–2%) and H_2 (2–14%) in He	–	$SCH_4 \cong 98\%$ (420 °C, $H_2/CO_2 = 7$, +0.4V)	–	–	[46]
Ru	YSZ disk (single chamber)	Impregnation	200–340 °C, 6NL/h, ±2V CO_2 (0.5–2%) and H_2 (0.1–15%) in He		$SCH_4 \cong 80\%$ (+2V) $SCH_4 \cong 54\%$ (-2V) (315 °C, $H_2/CO_2 = 7$)	$rCH_4 \cong$ 5.3 E−08 (+2V)		
	Na-ß-Al_2O_3 disk (single chamber)				– (315 °C, $H_2/CO_2 = 7$)	$rCH_4 \cong$ 0.5 E−07 (+2V) $rCH_4 \cong$ 0.2 E−07 (-2V)		
Pt	K-ß-Al_2O_3 candle (bipolar single chamber)	Dip-coating	400 °C, 90/522NL/h, −3 to 3V CO_2 (19.9–49.9%) and H_2 (49.9–79.9%) N_2 balance (0.5%)	1	$SCH_4 \cong 32\%$ (522 NL/h, 3V)	–	–	[65]
				2.5	$SCH_4 \cong 18\%$ (90 NL/h, 2V) (400 °C, $H_2/CO_2 = 1$)	–	–	
				10	$SCH_4 \cong 90\%$ $SCO \cong 10\%$ (400 °C, $H_2/CO_2 = 2$, 522NL/h, +3V)	–		
Pt	YSZ tube (bipolar single chamber)	Dip-coating	400 °C, 90NL/h, −2 to 2V CO_2 (19.9–49.9%) and H_2 (49.9–79.9%) N_2 balance (0.5%)	25	$SCH_4 \cong 32\%$ ($H_2/CO_2 = 2$, 0.5V)	–	–	[67]
Ru	BZY disk (single chamber)	Impregnation	350–450 °C, 12NL/h, −1 to 1V CO_2 (0.25–2.5%) and H_2 (1–15%) in He	–	$SCH_4 \cong 20\%$ (+1V, 450 °C) $SCH_4 \cong 54\%$ (-1V, 450 °C) ($H_2/CO_2 = 7$)	$rCH_4 \cong$ 1.5 E−07 (+1V, 400 °C)	500	[47]
Ni	K-ß-Al_2O_3 disk (single chamber)	Ni+α-Al_2O_3 paste	340-300 °C, 1.2–12NL/h, −2 to 2V CO_2 (1,5–10%) and H_2 (3–30%) in N_2	–	$SCH_4 \cong 40\%$ (2V, $H_2/CO_2 = 20$, 300 °C, 1.2NL/h)	$rCH_4 \cong$ 1.5 E−05	–	[56]
Ru–Co	BZY disk (single chamber)	Impregnation	250–475 °C, 12NL/h, −1.5 to 1.5V CO_2 (1%) and H_2 (7%) in He	–	$SCH_4 \cong 60\%$ (+1.5V, 450 °C) $SCH_4 \cong 68\%$ (−1.5V, 450 °C)	$rCH_4 \cong$ 0.6 E−07 (+1.5V, 450 °C) $rCH_4 \cong$ 0.4 E−07 (−1.5V, 450 °C)	47	[58]
Ru	YSZ disk (single chamber)	Impregnation	280–380 °C, 18NL/h, −2 to 1V CO_2 (1%) and H_2 (7%) in He	–	$SCH_4 \cong 80\%$ (340 °C, +1V)	$rCH_4 \cong$ 1.4 E−07	700	[49]
Ru	YSZ (monolithic type)	Sputtering	220–370 °C, 15–150NL/h, −2.5 to +2.5V CO_2 (1%) and H_2 (7%) in He	32	$SCH_4 = 92\%$ (60NL/h, 370 °C, +2.5V)	$rCH_4 \cong$ 26 E−07	5	[50]

Ru/Fe-oxide nanowires	YSZ disk (single chamber)	Impregnation	300–400 °C, 6NL/h, −1.5 to +1.5V CO_2 (1.5%) and H_2 (1.5–10.5%) in He	– – – –	100% CO 100% CO (400 °C, $H_2/CO_2 = 1$) 100% CO 100% CO (400 °C, $H_2/CO_2 = 7$)	rCO≅ 0.2 E−07 at +1 mA rCO≅ 0.3 E−07 at -1mA rCO≅ 0.37 E−07 at +1 mA rCO≅ 0.35 E−07 at -1mA	1 0.6 2.2	[60]
Ru	YSZ (O^{2-}) tube (Fuel cell type)	Impregnation	200–460 °C, 12–24NL/h, −1 to +1V CO_2 (1/3%) and H_2 (7%) in He	20 23	SCH_4≅70% (24NL/h, 450 °C, $H_2/CO_2 = 7$, -1V) SCH_4≅98% (24NL/h, 400 °C, $H_2/CO_2 = 7 + 0.1$V)	rCH_4≅ 2.1 E−07 rCH_4≅ 3.3 E−07	≅50 ≅500	[51]
Ru	BZY disk (single chamber)	Impregnation	350–400 °C, 6-24NL/h, −1 to 1V CO_2 (0.25–2.5%) and H_2 (1–15%) in He	–	SCH_4≅50% (+0.5V, 350 °C, $H_2/CO_2 = 4$) SCH_4≅60% (+0.5V, 400 °C, $H_2/CO_2 = 7$)	rCH_4≅ 1.4 E−07 (+0.5V, 400 °C, $H_2/CO_2 = 7$)	–	[48]
	YSZ disk (single chamber)		320 °C, 6-24NL/h, −1 to 1V CO_2 (0.25–2.5%) and H_2 (1–15%) in He	–	SCH_4≅45% (+1V, $H_2/CO_2 = 4$) SCH_4≅80% (+1V, $H_2/CO_2 = 7$)	rCH_4≅ 2.3 E−07 (+1V, $H_2/CO_2 = 7$)	–	
	K-ß-Al_2O_3 disk (single chamber)		350 °C, 6-24NL/h, −1 to 1V CO_2 (0.25–2.5%) and H_2 (1–15%) in He	–	SCH_4≅93% (−0.15V, $H_2/CO_2 = 4$) SCH_4≅80% (−0.15V, $H_2/CO_2 = 7$)	rCH_4≅ 2.3 E−07 (−0.15V, $H_2/CO_2 = 7$)	–	
	Na-ß-Al_2O_3 disk (single chamber)		320 °C, 6-24NL/h, −1 to 1V CO_2 (0.25–2.5%) and H_2 (1–15%) in He	–	SCH_4≅82% (−0.4V, $H_2/CO_2 = 4$) SCH_4≅88% (+0.2V, $H_2/CO_2 = 7$)	rCH_4≅ 0.2 E−07 (+0.2V,$H_2/CO_2 = 7$)	–	
Ru Co_3O_4 Ru/Co_3O_4	BZY disk (single chamber)	Impregnation	250–450 °C, 6NL/h, −1 to 1 mA CO_2 (1%) and H_2 (1–7%) in He	–	–	rCH_4≅ 0.2 E−07 (Ru, 1 mA, 400 °C, $H_2/CO_2 = 4$)	–	[54]
Fe-oxide nanowires	YSZ disk (single chamber)	Impregnation	300–400 °C, 6NL/h, CO_2 (1.5%) and H_2 (1.5%) in He	–	100% CO	rCO≅ 1 E−08 (1 mA, 400 °C)	–	[59]
Pt	YSZ (O^{2-}) tube (Fuel cell type)	Impregnation	260–460 °C, 6–24NL/h, −2 to +2V CO_2 (1%) and H_2 (7%) in He	≅12	100% CO	rCO≅ 1.7 E−07 (450 °C, $H_2/CO_2 = 7$, -2V)	–	[40]
Fe/TiO_2	YSZ tube (bipolar single chamber)	Dip-coating	225–400 °C, 90–216NL/h, −2 to 2V CO_2 (19.9–33.2%) and H_2 (66.3–79.6%) N_2 balance (0.5%)	≅5.5	SC_3H_6≅40% (325 °C, $H_2/CO_2 = 4$, 90NL/h, −0.5V)	–	≅1600	[68]

(continued on next page)

Table 1 – (*continued*)

Catalyst	Electrolyte/ configuration	Coating method	Operating conditions	XCO_2 (%)	Selectivity	Rate (mol/s)	$\|\Lambda\|_{max}$	Ref.
Ru	YSZ disk (single chamber)	Impregnation	250 °C, 6NL/h, 50 μA CO_2 (1%) and H_2 (7%) in He	–	–	$rCH_4 \cong$ 0.4 E−07	34	[53]
Cu NPs	YSZ disk (single chamber)	Impregnation	250–450 °C, 6NL/h, −1.5 −+2.5V	–	100% CO (450 °C, +2V, $H_2/CO_2 = 1$)	$rCO \cong$ 1.5 E−07	4.14	[63]
			CO_2 (0.1–1%) and H_2 (1–6%) in Ar	–	100% CO (400 °C, +2V, $H_2/CO_2 = 3$)	$rCO \cong$ 0.6 E−07	6.03	
				–	100% CO (400 °C, +2V, $H_2/CO_2 = 6$)	$rCO \cong$ 1 E−07	4.99	
Ni NPs	YSZ disk (single chamber)	Impregnation	360–420 °C, 18NL/h, −2 to 1V CO_2 (1–3%) and H_2 (1–7%) in He	–	100% CO	$rCO \cong$ 1 E−08 (420 °C, $H_2/CO_2 = 4$, O.C.)	–	[57]
Ru	YSZ (monolithic type)	Sputtering	370 °C, 60NL/h, −2.5/+2.5V CO_2 (0.2–4%) and H_2 (1 −12%) in He	≅39	$SCH_4 = 80\%$ (+2.5V, $H_2/CO_2 = 4$)	$rCH_4 \cong$ 30 E−07	≅3	[52]
				≅12	$SCH_4 = 68\%$ (−2.5V, $H_2/CO_2 = 4$)	$rCH_4 \cong$ 8 E−07	≅2	
Cu/Co_3O_4	YSZ disk (single chamber)	Impregnation	200–400 °C, 6NL/h, -1–+2V CO_2 (0.3–1%) and H_2 (1–6%) in Ar	–	100% CO	$rCO \cong$ 0.6 E−07 at +2V	190	[64]
				–	100% CO (400 °C, $H_2/CO_2 = 1$)	$rCO \cong$ 1.4 E−07 at -1V		
				–	100% CO	$rCO \cong$ 1.2 E−07 at +2V	175	
				–	100% CO (400 °C, $H_2/CO_2 = 6$)	$rCO \cong$ 1.9 E−07 at -1V		
PdZn	K-ß-Al_2O_3 disk (single chamber)	Impregnation	300–340 °C, 3.6–9.6NL/h, −2 to 2V CO_2 (0.25–2.5%) and H_2 (1 −15%) in He	0.1	$SCH_3OH \cong 60\%$ $SCO \cong 40\%$ (+2V, $H_2/CO_2 = 9$, 300 °C, 7.2NL/h)	$rCH_3OH \cong$ 0.9 E−07 $rCO \cong$ 9 E−07	250	[61]
	Na-ß-Al_2O_3 disk (single chamber)			–	– (-0.5V, $H_2/CO_2 = 9$, 300 °C, 7.2NL/h)	$rCH_3OH \cong$ 7.2 E−05 $rCO \cong$ 1.8 E−06	–	
Cu	K-ß-Al_2O_3 candle (bipolar single chamber)	Electroless	200–400 °C, 90/522NL/h, −2 to 4V CO_2 (19.9–33.2%) and H_2 (66.3–79.6%) N_2 balance (0.5%)	≅3	$SC_2H_6O \cong 45\%$ (325 °C, $H_2/CO_2 = 3$, 90NL/h, −0.5 V)	–	–	[66]
Cu	BZCY (co-ionic H^+ & O^{2-}) candle (bipolar double chamber, SOEC)	Electroless	325–550 °C, 42NL/h, −2 to 4V CO_2 (19.9) and H_2 (79.6%) N_2 balance (0.5%)	32.5	$SCH_4 = 94.2\%$ (450 °C, $H_2/CO_2 = 4$, 42NL/h, −0.5 V)	$rCH_4 \cong$ 9.2 E−07	5.5	This work

supported Cu on YSZ [64]. The main products obtained in these studies were methane and carbon monoxide, except in some cases where hydrocarbons, such as C_2H_4 over Cu on TiO_2-YSZ [38], and alcohols, such as CH_3OH over PdZn on Na-βAl_2O_3 or K-βAl_2O_3 [61] were also obtained. Among these studies the higher values of CO_2 conversion (about 40%) and selectivity to methane (almost 100%) were reported for the CO_2 hydrogenation over Cu on TiO_2-YSZ [38]. Moreover, most of these studies were carried out at laboratory scale and low gas flow rates, and using reactor configurations (discs), costly metals (Pt, Pd, Ru, Rd, etc.), metal film preparation methods (organometallic paste deposition or impregnation) and simplified gas compositions (H_2 and CO_2 diluted in He or N_2) which are not representative of the potential practical application of the technology to real CO_2 capture exit streams and renewable electrolytic hydrogen.

Some works reported the study of CO_2 hydrogenation over Ru [50,52] and Rh, Pt or Cu–TiO_2 [38] deposited by sputtering on YSZ in a potentially scalable monolithic electropromoted reactor (MEPR) under realistic operating conditions of pressure, temperature and flowrate, which represent an inestimable contribution to advance in the practical application of the technology. However, Ru, Rh and Pt are expensive noble metals and, in spite of using a cost-effective metal, the study of electrochemically enhanced CO_2 hydrogenation on Cu–TiO_2/YSZ [38] was still carried out using H_2 and CO_2 mixtures diluted in Helium and relatively high H_2/CO_2 ratios.

We have reported various bench-scale studies of electrochemically assisted CO_2 hydrogenation to valuable hydrocarbon and oxygenated fuels over Pt [65] and Cu [66] on K-βAl_2O_3, over Pt, Ni and Pd on YSZ [67] and on Fe–TiO_2 on YSZ [68]. These studies were carried out at high gas flow rates, under atmospheric pressure, at relatively low temperature and using gas compositions representative of CO_2 capture exit streams and tubular configurations easily adaptable to the existing catalytic devices (conventional flow reactors) and prepared by readily scalable procedures. In this work, the study of CO_2 methanation over Cu on BZCY, a co-ionic (H^+ and O^{2-}) and electronic (e^-) conductor, is addressed. Copper has been chosen as electrocatalytic metal film, in spite that only CO and H_2O are reported to be formed during the gas phase thermocatalytic methanation of CO_2 over conventional copper catalysts [69], because copper is not as prone to reoxidation or to catalyse coke formation as nickel [26]. In addition, copper is well known as one of the scarce efficient metals for the aqueous electrochemical reduction of CO_2, mainly to CH_4, at atmospheric pressure [70–72]. This unique feature of copper is related to the fact that Cu exhibits moderate binding energy with the adsorbed CO reaction intermediate resulting from CO_2 surface activation. The subsequent reduction of the adsorbed CO intermediate determines the selectivity to CH_4, as moderate binding energies are required for the formation of multi-electron products such as CH_4, i.e. too weak or strong binding energies can result instead in CO desorption or hydrogen evolution, respectively, from the copper surface [72]. In addition, the binding energy of the adsorbed CO intermediate over Cu, i.e. the relative CO surface coverage, can be modulated by varying applied potential [32] during the electrochemically assisted CO_2 hydrogenation to considerably enhance CH_4 selectivity, as demonstrated previously by Papaioannou et al. [38].

Unlike most previous studies in which electrochemically assisted catalytic hydrogenation of CO_2 was performed at a laboratory scale, this work has been carried out at an intermediate scale (bench scale) between laboratory and pilot plant. In general, the scale-up of a chemical process is carried out in five consecutive steps: laboratory, bench, pilot, semi-industrial and industrial. The concept of scaling-up refers to the change from one scale to another, by stepwise approaching the size, configuration and operating regime of the process unit to those required for its potential industrial application, in the course of the process research and development. Unlike laboratory scale, bench scale research is less fundamental and more technological and is carried out in an experimental setup (including feeding, preheating, reaction, control and data acquisition and gas analysis sections and enabling long-term continuous operation) and equipment (easily scalable monolithic or tubular reaction structures prepared by readily scalable procedures) configurations and operating conditions (high gas flow rates, concentrated CO_2 and H_2 binary mixtures, stoichiometric H_2/CO_2 ratios, etc.) similar to those existing or recommended at industrial scale. Moreover, the bench scale entails a higher level of instrumentation and automation than the laboratory scale.

Therefore, this work presents, to the extent of our knowledge for the first time, a bench-scale study of CO_2 methanation at the cathode side of a tubular co-ionic (H^+ and O^{2-} ion conducting) solid oxide electrolyte cell (SOEC). Specifically, electrochemically assisted CO_2 hydrogenation to CH_4 was investigated over a non-precious, widespread and cost-effective Cu electrocatalytic film (cathode) coated by electroless on a commercial (CoorsTek Membrane Sciences) anode (Ni-BZCY)-supported solid electrolyte (BZCY) candle. The study was carried out under atmospheric pressure at relatively high flow rates and intermediate temperatures, and using realistic gas compositions and an easily-scalable tubular configuration as an approach to a potential practical application of the technology. This work aimed to identify the most appropriate operating conditions in order to increase energy efficiency in CH_4 formation by maximizing CO_2 conversion and selectivity to CH_4 and by minimizing energy input in CH_4 formation, that is to say to maximize Faradaic efficiency, and also to minimize selectivity to CO and thus to reduce methane purification costs. Therefore, this study may contribute to fulfil the main key challenges for advancing CO_2 hydrogenation to fuels.

On the other hand, Kyriakou et al. [73] have already studied hydrogen production by steam reforming at the anode side (Ni-BZCY) of a similar cell reactor (Ni-BZCY/BZCY/Cu) and simultaneous separation of hydrogen through the BZCY solid electrolyte membrane, which may contribute to speed the development of the proposed tubular co-ionic SOEC for the in-situ production of methane from CO_2 and renewable hydrogen and energy sources.

2. Material and methods

2.1. Experimental set-up

The Cu/BZCY/Ni-BZCY electrochemical cell evaluated in this work consisted of a thin Cu electrocatalytic film (cathode)

deposited on the outer surface of a 10-mm-i.d., 100-mm-long, and 1-mm-thick anode (Ni-BZCY72)-supported solid electrolyte (BZCY72) tube (CoorsTek Membrane Sciences), closed at one end to enable the set-up of a double-chamber cell configuration. The Ni-BZCY anodic electro-catalyst was considered appropriate because it has been reported to be a highly active support [73]. The Cu cathode was chosen as working electrode because it is known to be effective in reactions involving reduction of CO such as methanol synthesis, RWGS or hydrogenation of CO_2 [73,74].

The copper layer was coated on the outside surface of the anode-supported BZCY tube by electroless deposition method, because it has been reported to improve cell performance [75] compared to Cu electrodes coated via conventional plating by depositing an organometallic paste of Cu on top of the solid electrolyte membrane [73,76]. However, Patki et al. [77,78] showed that Cu electrodes fabricated using pastes are thick (typically 10–20 μm), present poor adhesion to the BZCY electrolyte, are prone to delamination and exhibit an unstable microstructure on high temperature heat treatment. This work made use of the electroless method [79–83], an autocatalytic chemical technique that allows the deposition of a metallic film on top of insulating or conducting solid workpieces without the use of an external electrical power supply. Therefore, this technique is pertinent to non-conductive ceramic substrates, such as electrolytes. Electroless was chosen because of the various advantages it presents over other deposition techniques: allows the deposition of very thin films of either one single metal or chemically similar metal alloys, over any substrate geometry and either outside or inside of a tubular support.

Substrates require previous activation by a catalyst, typically palladium, to initiate the deposition process. Copper, among other metals, is electrocatalytic, i.e., once deposition begins, the thickness of the film continues to increase.

On this occasion, the outer surface of the BZCY tube was first cleaned with a mix of methanol and acetone (50/50) and then activated with a thin Pt layer deposited by dip coating. Pt precursor solution was prepared in accordance with a CIEMAT European patent [84] following the procedure described in detail elsewhere [65,67]. After platinum activation, the Cu film was deposited by electroless following the procedure described in detail in elsewhere [66]. To form the double chamber reactor configuration, once the cathode Cu film has been deposited, the tubular electrochemical cell was attached to a 110-cm long, 10-mm inside diameter, 1-mm thick quartz tube. The quartz tube was glued to the cell with a product specifically designed for ceramic materials (Ceramabond 569), but only after their surfaces were etched and smoothened with an abrasive sandpaper and cleaned both with ethanol and in a water bath with an ultrasound treatment for proper bonding of the materials. With these steps finished, and after 4 h of air drying, the whole quartz tube was installed inside a quartz reactor with 35.4 mm of diameter and 1150 mm of length. The annular space between the two quartz tubes conform the external cell chamber, which would then allow the injection of gases into the internal chamber (Ni-BZCY anode) or annular chamber (Cu cathode) of the reactor. The double chamber reactor was placed in a concentric three-zone electrical furnace integrated in a bench-scale plant, described in detail elsewhere [65], which is able to process up to 20 Nm^3/h of gas with temperatures up to 900 °C and at atmospheric pressure. Afterwards, the cell underwent two heat treatments of 2 h each for curing the glue: the first one conducted at 95 °C and the second one at 260 °C (with an increasing heating ramp of 5 °C/min and 1 °C/min, respectively).

It must be stated that due to the previous thermal treatments conducted, the electrocatalysts underwent an oxidation process. When oxidized, electrical conductivity of the electrodes decreases, so a reduction process was implemented by injecting hydrogen into the reactor. 700 NmL/min and 170 NmL/min of H_2 were respectively fed into the external and internal chamber of the reactor at 450 °C for 4 h.

After reduction, the electrical resistance of the cell was measured and accounted for a value of 380 Ω, added to the fact that the colour of the Cu catalyst turned back to its initial one; both being factors of adequate electrical conductivity of the electrodes.

Both cathode (Cu) and anode (Ni-BZCY) electrodes were connected to a potentiostat-galvanostat (Voltalab 21) through two different stainless steel wires to allow the induction of voltage potentials across the electrochemical cell.

Gases used in the experiments were fed from compressed-gas bottles (Air Liquide) and were metered by a battery of electronic mass flow controllers (Brokhorst High-Tech). Gas samples were analysed using a gas micro-chromatograph (Varian CP- 4900). The sampling line from the reactor exit to the gas micro-CG was heated to avoid potential condensation of any volatile products.

The gas micro-GC was equipped with automatic injectors and three column modules attached to the corresponding micro thermal conductivity detector (micro TCD) which enabled the analysis of H_2, N_2, CO, CH_4, CO_2 and various light hydrocarbons and oxygenates. Helium was used as reference and carrier gas.

2.2. *Catalyst characterisation*

The cross-section and the outer (Cu film cathode) surface of the Cu/BZCY/Ni-BZCY electrochemical cell were characterised, both as prepared (after Cu deposition and calcination in air for sealing the tube) and after H_2 reduction and testing, by Scanning Electron Microscopy (SEM) coupled to Energy Dispersive X-ray spectroscopy (EDX), X-Ray Diffraction (XRD) and X-ray Photoelectron Spectroscopy (XPS) techniques described previously elsewhere [66].

The morphology and thickness and surface Cu distribution of the Cu film were examined via SEM-EDX by means of a HITACHI S-2500 instrument of 35 Å of resolution and 25 kV of accelerating voltage.

Diffractograms of the Cu film were recorded on a PHILIPS "Xpert-MPD" apparatus utilizing a Cu Kα X-ray source (40 mA and 45 kV), a step time of 2 s, a 2θ range of 15–75° and a step size of $2\theta = 0.03°$.

The average crystallite size of the copper film was estimated from X-ray line broadening analysis of the main diffraction peak of metallic Cu for the reduced sample, by the Debey-Scherrer equation (1) [85–88]:

$$d_c = \frac{K\lambda}{\beta \cos\theta} \quad (1)$$

Where d_c is the Cu crystallite diameter in nm, K is a constant known as the shape factor which usually takes the value of 0.9, λ is the incident X-ray wavelength in nm, β is the width at half height (FWHM) of the most intense XRD peak of Cu metal in radians and θ is the diffraction angle in degrees.

The metallic dispersion of the Cu cathode film was estimated using equation (2) [85].

$$D = \frac{1.1}{d_c} *100 \quad (2)$$

Where *D* is the metal dispersion expressed in percentage and d_c is the Cu crystallite diameter obtained from equation (1) in nm.

The surface chemical composition of the Cu film was analysed via XPS by a PerkinElmer PHI 5400 System with a beam diameter of 1 mm and a Mg Kα ($h\nu = 1253.6$ eV) excitation source (20 mA and 15 kV). Base pressure in the analytical chamber was about 10^{-9} Torr. The step energy was 89.5 eV for broad spectra (0–1100 eV) and 35.75 eV for high resolution spectra. The energy scale was referenced to the carbon 1s signal at 285.0 eV.

2.3. Operating conditions and procedure

The Cu cathode film was previously reduced in H_2 at 450 °C for 4 h and then tested at atmospheric pressure and under a binary gas mixture with a H_2 to CO_2 molar ratio of 4, as required by the stoichiometry of the methanation reaction, and a flow rate of 42 NL/h. CO_2 gas characteristics simulated those of a CO_2 capture amine scrubbing industrial process (>99% purity), while H_2 simulated the ones obtained from a renewable process such as electrolysis (>99% purity). A diluted H_2 (10% v/v H_2 in N_2) stream (6 NL/h) was fed to the inner anode chamber as a source of H^+ promoter ions and to avoid the Ni anode from oxidizing.

Firstly, open circuit experiments were performed, under temperature programmed manner, in order to identify a suitable operating temperature, by following the effect of temperature (between 325 and 550 °C) on CO_2 conversion and selectivity to the different products (mainly CH_4 and CO) under un-promoted conditions. Then, potentiostatic electropromoted tests were performed to investigate the steady state influence of polarization on the behaviour of the electrocatalysts in closed circuit configuration. Open circuit potential was maintained during 30 min prior to each test to define a reproducible reference state. The effect of polarization (under application of constant potentials from 2 to −2 V with a 0.5V step decrease) on catalyst performance was investigated at the temperature selected from the temperature programmed tests (450 °C). The carbon mass balance (relative difference between carbon mass at the reactor inlet and outlet) was calculated for each test to gauge potential coke deposition. The error closing the carbon mass balance resulted to be lower than 3%.

A small quantity of N_2 (around 0.5%) was also added to the H_2 and CO_2 binary mixture as an internal standard to balance subsequent calculations. Accordingly [65], equation (3) was applied to determine CO_2 conversion (X_{CO_2}).

$$X_{CO_2} = \left(1 - \frac{[CO_2]_o \times [N_2]_i}{[CO_2]_i \times [N_2]_o}\right) *100 \quad (3)$$

Where $[CO_2]_i$ and $[CO_2]_o$ are the CO_2 molar concentrations at the inlet and outlet of the cathodic chamber. Analogously, inlet and outlet molar concentrations of N_2 are represented by $[N_2]_i$ and $[N_2]_o$.

Selectivity of the different products generated in the reaction, known as "CO_2 free selectivity", was defined [65] as (4):

$$S_i = \left(\frac{c_i * M_i}{\sum_{j=1}^{j=n} c_j \times M_j}\right) *100 \quad (4)$$

Where "S_i" is the selectivity, "c_i" is the number of carbon atoms and "M_i" is the molar flow of product i, respectively and "*n*" is the number of different products formed.

To obtain the catalytic rate of CO_2 the following equation (5) was considered:

$$rCO_2 = \frac{(Q_{CO_2} * X_{CO_2})/100}{22414*60} \quad (5)$$

Where rCO_2 is the catalytic rate in mol/s of the conversion of CO_2, Q_{CO_2} is the flow rate in NmL/min of CO_2 injected into the system considering the utilized H_2/CO_2 ratio of 4, and 22141 is the molecular volume of a gas in NmL/mol.

From (5), the catalytic rate of formation of any product generated in the reaction could be calculated as in (6):

$$r_i = \frac{rCO_2 * S_i}{100} \quad (6)$$

Where, r_i is the catalytic rate of formation of product i in mol/s and rCO_2 and S_i are obtained from (5) and (4), respectively.

The effect of polarization on catalyst performance for the CO_2 methanation reaction was evaluated in terms of the rate enhancement ratio [65] defined as (7) and the apparent Faradaic efficiency or NEMCA (Non faradaic Electrochemical Enhancement of Catalytic Activity) enhancement factor Λ [38,68] defined from (8).

$$\rho_i = \frac{r_i}{r_{io}} \quad (7)$$

$$\Lambda_i = \frac{(r_i - r_{io}) * E_i}{I/F} = \frac{\Delta r_i (mol/s) * E_i}{I/F} \quad (8)$$

Where r_i is the electropromoted rate (under application of a given potential V) and r_{io} is the unpromoted catalytic rate under open circuit conditions (without potential application) of the corresponding product formation. F is the constant of Faraday (96485C/mol), I is the applied current, Δr_i is the current- or potential-induced variation in the catalytic rate (mol/s) and E_i is the g-eq factor for each product formation reaction. The Faraday's law predicts Δr_i in g-eq/s and a g-eq is equal to the molecular weight of the compound formed divided by the number of electrons transferred. In this way, the number of g-eq can be represented as moles multiplied by the number of electrons transferred. Therefore, E_i can be calculated as the number of electrons transferred divided by the stoichiometric coefficient in each product formation reaction. In this study, Λ has been calculated for the target product (methane)

formation (Λ_{CH4}), i.e. $E_{CH4} = 8$, according to the stoichiometry of the CO_2 methanation reaction. The term I/F relates to the rate of ions (g-eq/s) transferred according to the Faraday's law. Thus, $|\Lambda| = 1$ denotes pure Faradaic rate enhancement, and $|\Lambda| > 1$ indicates electrochemical promotion. Although reactions conducted here are governed by non-faradaic processes –because of the electrochemical promotion effect and violation of Faraday's laws– Faradaic efficiency is still obtained to provide an idea of the energy efficiency of the methanation process. The Faradaic efficiency (η_c) and the energy cost (C_E) were calculated for the CO_2 methanation reaction upon different applied potentials, following equations (9) and (10) [68], correspondingly:

$$\eta_c = \left\{ \left(m_p / M_p \right) * \nu_e / \nu_p * F \right\} \Big/ (I * t) \quad (9)$$

$$C_E = V * \left(\nu_e / \nu_p \right) * F \Big/ \left(\eta_c * M_p \right) \quad (10)$$

Where, ν_e is the number of electrons conveyed and ν_p is the stoichiometric coefficient in formation reaction of each product (i.e. for the CH_4 formation reaction $\nu_e = 8$ and $\nu_p = 1$). Moreover, M_p and m_p are the molecular weight and mass of product each formed, respectively.

3. Results and discussion

3.1. Catalyst characterisation studies

SEM micrographs of the Cu cathode surface, both as deposited and after reduction and testing, are shown in Fig. 1a and b, respectively. A SEM micrograph of the interface between the Cu cathode film and the BZCY solid electrolyte is shown in Fig. 1c as prepared. The Cu film thickness can be assessed from Fig. 1c and resulted to be between 1.1 and 1.5 μm.

In order to give an idea of the level of Cu dispersion, an EDX mapping of the Cu distribution in the as prepared Cu porous film is shown in Fig. 2.

Therefore, it can be stated that the utilized electroless technique enabled the deposition of a porous resembling and very thin Cu film (<2 μm), rendering a low surface electrical resistance (below 1 Ω) and enhanced proton and oxygen ion transfer to or from the catalyst surface and reactant/product diffusion, which make it suitable for the electro-catalytic tests [89].

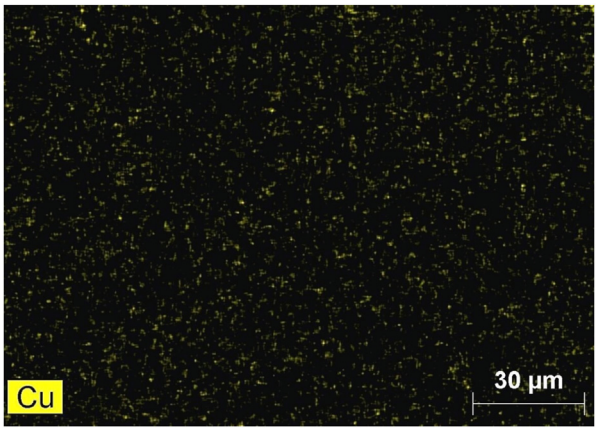

Fig. 2 – EDX mapping of Cu surface distribution in the as prepared Cu film.

The Cu film seems to exhibits also good adhesion with the BZCY electrolyte given that it is continuous, as can be derived from the SEM micrograph of the interface between the Cu cathode film and the BZCY solid electrolyte (Fig. 1c) and as verified by electrical conductivity measurements. XRD patterns of the Cu cathode film, both as prepared (after Cu deposition and calcination in air for sealing the tube) and after reduction and testing, are depicted in Fig. 3a and b, respectively.

The peaks at around $2\theta = 43.3$, 50.45, 74.1 and 89.9 in the used (after H_2 reduction and testing) sample were identified as diffraction peaks of metallic Cu (JCPDS card no. 01-085-1326); whereas the peaks at about $2\theta = 29.6$, 36.5, 42.4, 52.6, 61.55, 69.79, 77.6 and 85.2 in both samples can be ascribed to Cu_2O (JCPDS card no. 01-077-0199). Upon reduction and testing, a shift in the peaks associated to Cu oxides to $2\theta = 36.6$, 42.6, 61.7 and 77.9 is observed, which may be ascribed to the presence of CuO (JCPDS card no. 01-078-0428).

The average crystallite size of the Cu film was around 42 nm, as calculated (1) from X-ray broadening of the main diffraction peak of metallic Cu (Cu (111) reflection at

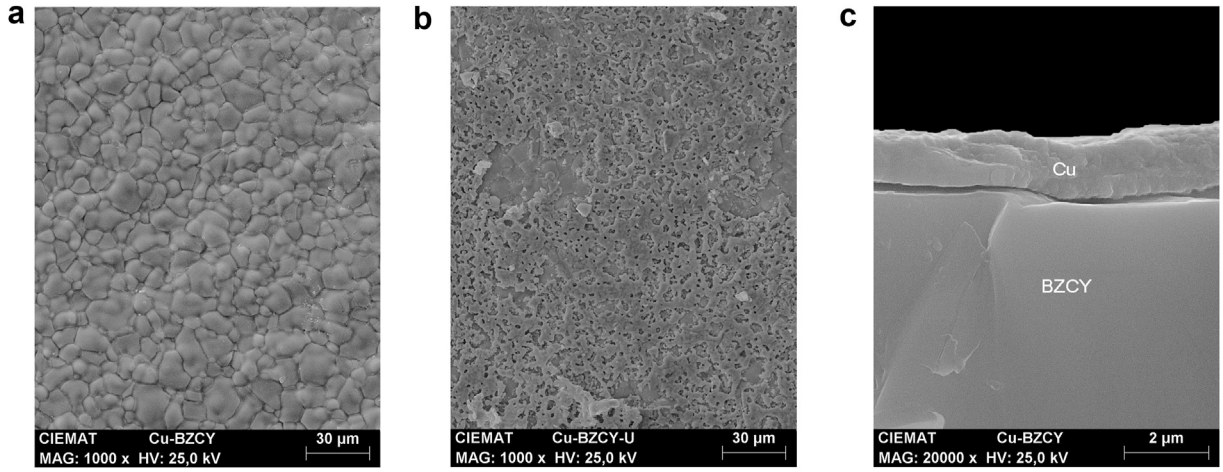

Fig. 1 – SEM micrographs of the Cu cathode: (a) surface as prepared, (b) surface after reduction and testing and c) Cu film.

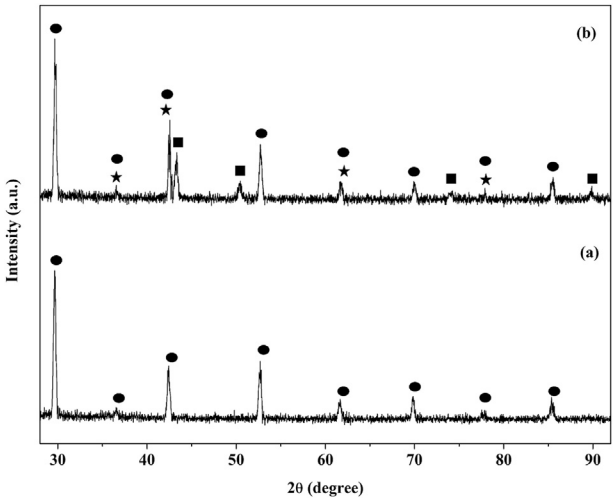

Fig. 3 – XRD analysis of the Cu cathode film: (a) as prepared and (b) after reduction and testing. Cu° (■), Cu_2O (●) and CuO (★).

2θ = 43.317) via the Debey-Scherrer equation [85–88]. The metal dispersion of the Cu cathode film has been also estimated (2) from the obtained crystallite diameter and resulted to be of approximately 2.6% [85].

The Cu loading (total quantity of metallic Cu coated) was about 0.025 g. The electrochemical active surface area (mol of active sites) of the Cu cathode film was calculated [55] from metal dispersion and Cu loading and was about 1.02×10^{-5} mol Cu.

XPS spectra of the Cu cathode film, both as prepared and after reduction and testing, are also shown in Fig. 4a and b, respectively.

XPS analysis of the as prepared Cu film made evident the presence of various surface compounds, resulting in Cu being present as 80.6% Cu_2O and 19.4% $CuO/Cu(OH)_2$, as shown by the appearance of peaks at binding energies of about 932.1 eV and 934.2/936.3 eV, respectively, in the Cu 2p3/2 spectra.

It seems that exposure of the Cu catalyst film to hydrogen and reducing testing gas environment resulted in an almost complete reduction of Cu oxide to metallic Cu, in accordance with XPS analysis of the used sample, resulting in almost all (94%) Cu being present in metallic form with a small amount (about 6%) of Cu remaining as Cu oxides as resembled by the appearance of peaks at binding energies of about 931.9 eV and 934 eV, respectively, in the Cu 2p3/2 spectra. The appearance of a peak at about 529.2 eV in the O1s spectra seems to confirm the presence of metal oxides (mainly CuO) in the as prepared and used samples. XRD results seem to confirm these findings as resembled by the appearance of characteristic diffraction peaks of metallic Cu in the used sample and the observed shift in the XRD peaks associated with Cu oxides after reduction and testing.

3.2. CO_2 hydrogenation tests

3.2.1. Effect of temperature

Firstly, open circuit (un-promoted) experiments were performed at temperatures between 325 and 550 °C in order to identify a suitable operating temperature. Results obtained from these tests are shown in Fig. 5.

As it can be appreciated in Fig. 5, the only products generated were CH_4 and CO. Selectivity to CH_4 clearly presents a higher value than that of CO, especially at temperatures between 350 and 400 °C (with a maximum of 97.34% at 400 °C); which corresponds to that reported in literature [38]. High selectivity to CH_4 was expected considering the ratio of 4 used, which was chosen according to the stoichiometry of the methanation reaction (11). However, such a high selectivity to methane is reported not be easily achieved [47,65], especially under open circuit conditions. Such high values may be explained by various factors. First, although no polarization was applied, a small potential difference was measured across the cell (0.128 V), which could have been caused by the different partial pressures of H_2 at separated sides of the cell and the distinct composition of the electrodes. In addition, it must be noticed that promoter ions can also thermally migrate from the electrolyte to the catalyst surface (or vice versa) due to the increased ionic conductivity of the electrolyte at high temperatures.

CH_4 was preferentially formed over CO on Cu/BZCY under the studied operating conditions. CH_4 selectivity slightly increased with temperature up to 400 °C, whereas CO_2 conversion exhibited a minimum at 450 °C. At higher temperatures, where methanation (exothermic) (11) and reverse water gas shift (endothermic) (12) reaction is thermodynamically retarded and favoured [90], respectively, CO selectivity starts to rapidly increase up to about 21% at 550 °C, while CH_4 one decreases to around 79%.

A temperature of 450 °C was finally selected for the subsequent potenciostatic tests in order to assure high values of electronic/co-ionic conductivity of BZCY and CH_4 yield. This value was chosen as a projective measure for future tests of CO_2 hydrogenation with in-situ H_2 production, since main H_2 production processes at the anode side of similar electrochemical cells based on BZCY co-ionic electrolytes, such as electrolysis [91] and reforming [73] are endothermic and thus favoured at higher temperatures. In fact, Kyriakou et al. [73], which studies low-temperature methane steam reforming in a double-chamber reactor at the anode side of the same electrochemical cell (Ni-BZCY/BZCY/Cu) as this paper, utilized an operating temperature range of 450–600 °C.

$$CO_2 + 4\,H_2 \rightarrow CH_4 + 2\,H_2O\ (\Delta Hr = -165\ kJ/mol) \quad (11)$$

$$CO_2 + H_2 \rightarrow CO + H_2O\ (\Delta Hr = +40\ kJ/mol) \quad (12)$$

3.2.2. Effect of potential

Fig. 6 shows the resulting effect of the applied potential on the conversion of CO_2 and formation of CH_4 and CO. As it can be appreciated in Fig. 6, there is a maximum in selectivity to CH_4 of 94.2% at −0.5 V; after 0.5 V it starts to drop, reaching a value of 90.9% at 2 V. CO_2 conversion presents a local minimum of 23.8% under open circuit conditions (about 0 V), but shows a rather progressive increase from 19.7% at −2 V to 32.5% at −0.5 V and from 32% at 0.5–34.7% at 2 V. Selectivity to CO remains almost constant around 6% until 0.5 V, where it starts to increase, reaching a maximum of 9.1% at 2 V. These

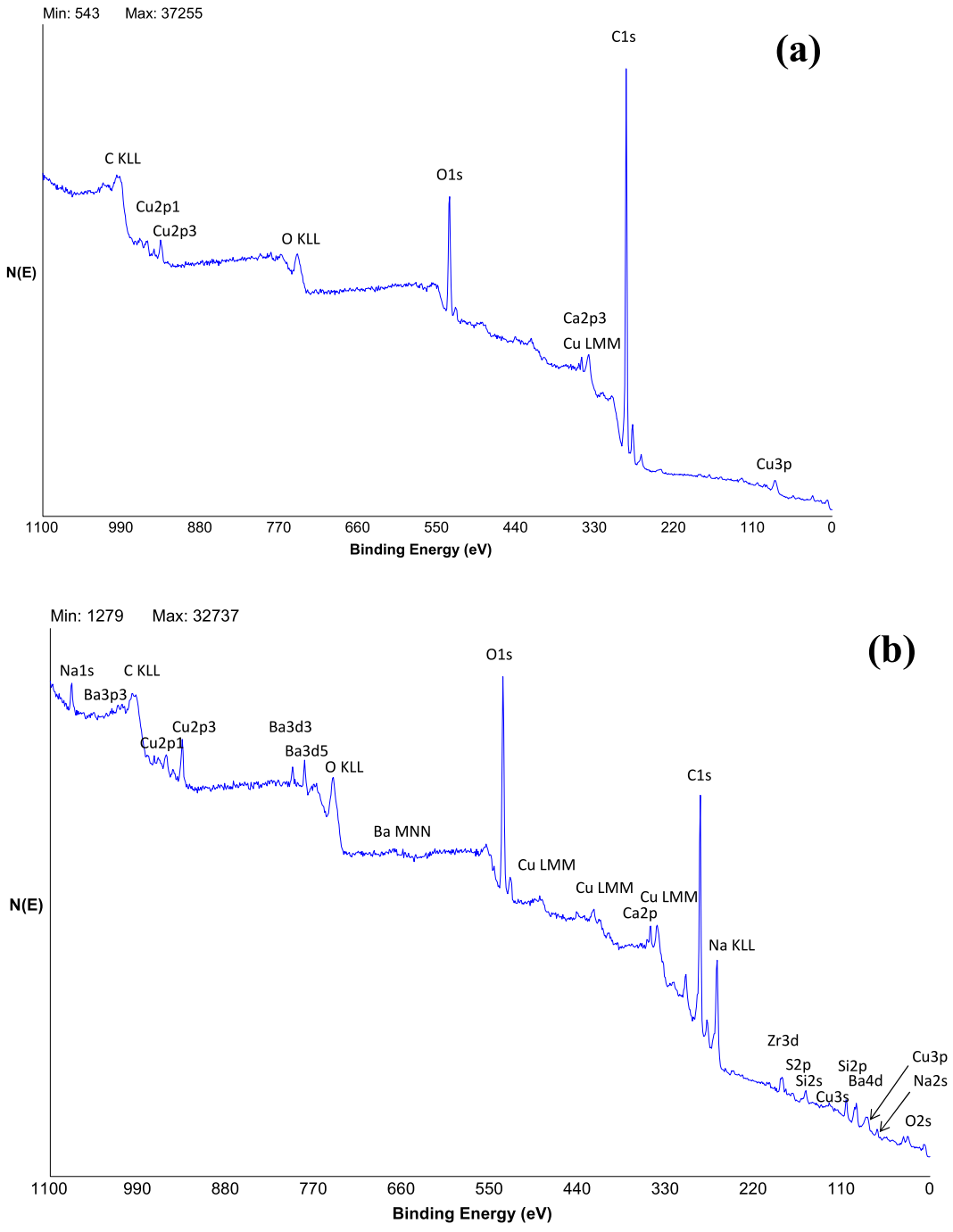

Fig. 4 – XPS spectra of the Cu cathode film: (a) as prepared and (b) after reduction and testing.

conversion and selectivity variations are explained by the migration of ionic promoters, which move across the electrolyte from the cathodic electrocatalyst to the anodic one (and vice versa) depending on the applied polarization. It must be pointed out that BZCY is a co-ionic electrolyte, so both oxygen ion (O^{2-}) and proton (H^{+}) promoters took part in the electropromoted phenomena.

With increasing positive potentials, the work function of the electrode increased by addition of O^{2-} promoters and removal of H^{+}, thus facilitating the adsorption of H_2; i.e., the electrode turns positively charged (because of a deficiency of electrons) and favours the transference of electrons from electron donor molecules (such as H_2) to the Cu catalyst, whereas simultaneously the adsorption of electron acceptor molecules (such as CO_2) is hindered. With increasing negative potentials, H^{+} promoters are pumped to and O^{2-} promoters are removed from the cathode surface, diminishing the work function of Cu and thus facilitating the chemisorption of CO_2 and inhibiting the adsorption of H_2; i.e., the electrode comes to be negatively charged (due to a surplus of electrons), favouring transference of electrons from the Cu catalyst to electron acceptor compounds (such as CO_2) and hindering the

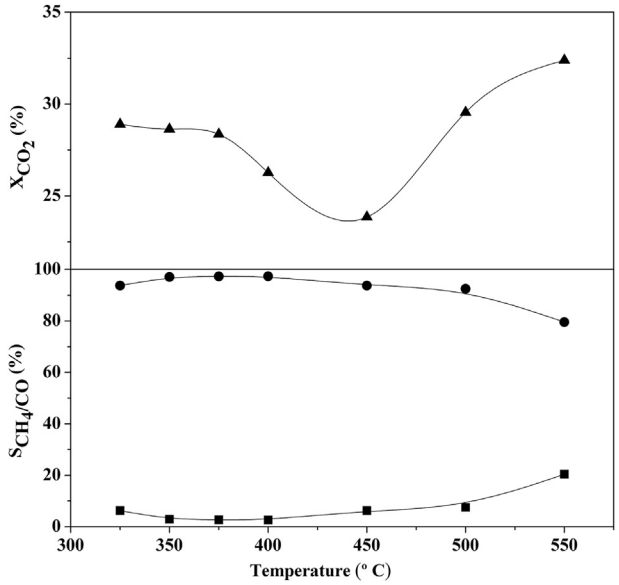

Fig. 5 – Influence of temperature on (▲) CO_2 conversion and on selectivity to (●) CH_4 and (■) CO over the Cu cathode film under open circuit conditions. (1 bar, 42 NL/h, $H_2/CO_2 = 4$).

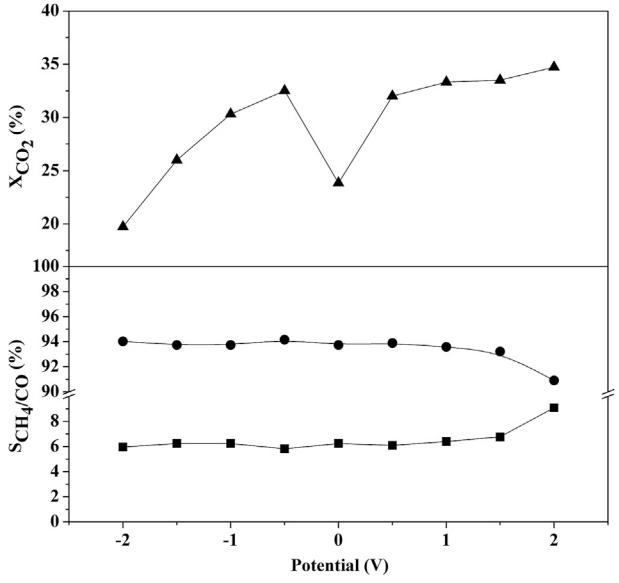

Fig. 6 – Influence of applied potential on (▲) CO_2 conversion and on selectivity to (●) CH_4 and (■) CO over the Cu cathode film. (1 bar, 42 NL/h, $H_2/CO_2 = 4$, 450 °C).

adsorption of electron donor ones (like H_2) [32,92]. In this manner, according to the relative electronegativity of the distinct adsorbates involved in the CO_2 methanation reaction and on which of them is in excess on the Cu catalyst surface, the applied polarization, and thus the removal or supply of H^+ and O^{2-} promoters to the Cu surface, might have beneficial or adverse effect on the overall methanation kinetics. Therefore, the displayed electrochemically promoted catalytic performance may be rationalized taking into account the influence of changing applied potential on the chemisorption strength of reactants, intermediates and products.

At negative potentials, pumping of H^+ to and removal of O^{2-} from the Cu cathode surface enhances CO_2 adsorption and activation, occasioning the formation of a very distorted CO_2 molecule (CO_2*) that interacts with the Cu catalyst surface (13) and forms a strong Cu–CO_2* bond [93,94].

$$CO_2 + e^- \rightarrow CO_2^{*-}\ (ads.) \tag{13}$$

Due to the removal of O^{2-} ions, negative polarization also strengthens the Cu–C bond and weakens the C–O bond, enhancing CO_2 dissociation to CO (14). Considering the rules of electrochemical promotion [38,44], CO dissociative adsorption is less favoured at negative potentials (CO has a lower electron acceptor capacity than CO_2), subsequently resulting in CO desorption (15) an in an increase in the selectivity to CO. However, in this case, CO selectivity appears to decrease at negative potentials, whereas CH_4 selectivity increases. This is explained by electrochemical semi-reactions taking place at the electrode surface which are favoured by O^{2-} removal from the catalyst; i.e. the weakening of C–O bond upon negative polarization also favours dissociation of CO (16) and CO_2 (17), via O^{2-} abstraction, into reactive surface carbon species C* over small Cu particles, resulting in a decrease in CO selectivity [95].

$$CO_2^{*-}\ (ads.) + e^- \rightarrow CO^*\ (ads.) + O^{2-} \tag{14}$$

$$CO^*\ (ads.) \rightarrow CO \tag{15}$$

$$CO^*\ (ads.) + e^- \rightarrow C^*\ (ads.) + O^{2-} \tag{16}$$

$$CO_2^{*-}\ (ads.) + 4\,e^- \rightarrow C^*\ (ads.) + 2\,O^{2-} \tag{17}$$

Taking into account reactions (16) and (17), it can be seen that negative polarization favours the formation of CH_4 precursor species (C*). In addition, under a stoichiometric H_2/CO_2 ratio of 4, hydrogen coverage at the electrode surface should be higher enough for C* adsorbed species (CH_4 precursor species) to be further hydrogenated to CH_4 as in (18) [85,95]. Moreover, despite hydrogen evolution reaction (19) (which may limit the CO_2 hydrogenation) is favoured at negative potential, pumping of H^+ to the Cu catalyst surface upon negative polarization may contribute also to an increased hydrogen surface coverage improving CO_2 methanation [28,37]. Thus, the reduction of CO species (16) (before desorption) or total CO_2 reduction (17) could be the reason for the observed behaviour at negative potentials.

$$C^*\ (ads.)\ (CH_4\ precursors) + O\ (ads.) + 6\,H\ (ads.) \rightarrow CH_4 + H_2O \tag{18}$$

$$2\,H^{*+}\ (ads.) + 2e^- \rightarrow H_2 \tag{19}$$

The application of positive potentials give rise to a migration of oxygen ions to the catalyst surface and a removal of H^+ from the catalyst surface, favouring H_2 (electron donor) dissociative adsorption (20) on the Cu surface and resulting in an increase of the surface coverage of hydrogen and in a decrease in CO_2 coverage, being CO_2 (electron acceptor) adsorption the reaction limiting step.

$$H_2 \rightarrow 2\,H^{*+}\,(ads.) + 2e^- \quad (20)$$

In addition, according to literature [96], at positive potentials CO_2 dissociative adsorption over Cu is thought to be improved by coadsorbed hydrogen (21). CO adsorbed species formed by CO_2 dissociation can desorb in the gas phase (15) or can be progressively hydrogenated resulting finally in CH_4 formation, expressed as (22).

$$CO_2^{*-}\,(ads.) + e^- + 2\,H^{*+}\,(ads.) \rightarrow CO^*\,(ads.) + H_2O \quad (21)$$

$$CO^*\,(ads.) + 6\,H\,(ads.) \rightarrow CH_4 + H_2O \quad (22)$$

Even though that the electropromoted experiments were carried out at a H_2/CO_2 ratio of 4 –which corresponds which that stoichiometrically required for CH_4 formation– at high positive potentials (higher H_2 adsorption region) hydrogen coverage should be higher than that of CO adsorbed species resulting from CO_2 dissociation, and, thus, the latter species gradually hydrogenated to CH_4, eventually resulting in an increment in CH_4 selectivity. However, on increasing potential, hydrogen is pumped away from the Cu catalyst surface, resulting in a lower hydrogen surface coverage and therefore in a decrease of CH_4 selectivity. Moreover, CO adsorption is also limited at high positive potentials (CO is a weaker electron donor than H_2) and it tends to desorb (15), which explains the increase in CO selectivity.

Although applied negative potentials enhance chemisorption of electron acceptor molecules and methane formation, it must be highlighted that excessive pumping of H^+ to the Cu catalyst surface can also inhibit CO_2 adsorption, which explains the decrease in CO_2 conversion. Therefore, in this work, at high negative potentials migration of H^+ to the catalyst represents an inhibiting factor for CO_2 conversion to CH_4. On the contrary, it can be seen that CO_2 conversion gradually increases with increasing positive potentials. This happens because, despite carbon dioxide adsorption being less favoured at positive potentials (due to O^{2-} pumping to the catalyst surface), a higher amount of hydrogen is adsorbed, thus increasing CO_2 conversion, either to CH_4 at lower potentials, or to CO at higher potentials due to excessive hydrogen removal from the surface, as explained previously.

Therefore, it can be reasonably concluded that there is a shift in methanation pathway upon switching from positive potentials (associative mechanism) to negative potentials (dissociative mechanism). The mechanism of thermocatalytic CO_2 methanation has been proposed to proceed through the formation of either intermediate species (HxCO), from the adsorbed CO generated by CO_2 dissociative adsorption, or surface carbon species (C*), by rupture of the C–O bond without intervention of CO as intermediate, and subsequent hydrogenation of the corresponding intermediate species to CH_4 [69]. In addition, two competitive pathways have been proposed for the CO_2 hydrogenation to methane on Cu based electrocatalysts, depending on applied potential [97]. The first one takes place through the sequential hydrogenation of adsorbed CO (CO*), deposited by the CO_2 dissociative adsorption, to CHO* (formyl) intermediate and finally to adsorbed methoxy intermediate CH_3O* [5,70–72,97]. Hydrogenation of the methyl group of CH_3O* results in the formation of CH_4. The second mechanism proceeds instead through progressive CO_2 electrocatalytic reduction to adsorbed CO (CO*) and finally, via COH* (hydroxymethylidyne) intermediate, to carbon surface species (C*) which are finally hydrogenated to CH_4 [5,71,72,97,98]. This route is also call as coking pathway as can result in coke formation.

Various studies have postulated that the first route proceeds from adsorbed CO (CO*) to CH_3O* through C–H bond formation via stepwise hydrogenation by surface adsorbed hydrogen species, resulting finally in CH_4 formation [70–72,97], which is consistent with the associative methanation mechanism proposed at high positive potentials (equations (20) to (22)), and that the selectivity to CH_4 results from the facility of the Cu (111) surface to concurrently house CO* and H^{*+} coverages [99,100]. At more negative potentials, the second route has been proposed to take place through the COH* intermediate via formation of a O–H bond, by protonation of CO*, and subsequent rupture of the C–O bond to give surface carbon species (C*) which are finally hydrogenated to CH_4 [71,72,97,98], which is consistent with the dissociative methanation mechanism proposed at negative potentials (equations (14) to (18)). These findings suggested the existence of a change in the nature of the CO_2 methanation mechanism from chemical, via reaction of coabsorbed CO and hydrogen, to electrochemical, via reduction of adsorbed CO by the protons pumped to the Cu surface, at a given value of applied potential [99].

To bring some evidence on the potentially formed surface carbon intermediate species, the Cu cathode film, both as prepared and after reduction and testing, was characterized by XPS. Three different types of carbon species were identified in the C 1s XPS spectra of both as prepared (Fig. 7a) and used (after reaction) (Fig. 7b) Cu samples.

The presence of carbon in the as prepared sample can be due to sample contamination or resulting from the used deposition procedure. The main XPS C 1s peak at binding energies around 284.75 eV, which could be attributed to graphitic-like carbon (C–C or C–H) [101,102], decreased in the used sample, indicating no substantial deactivation by coking [97]. Two additional shoulder peaks appear, together with the main peak, in the C 1s spectrum of the as prepared sample, at binding energies at about 288.18 and 286.35 eV which may be assigned as carboxylic groups (C=O) and ether groups (C–O), respectively. The increase in the contribution of both carboxylic (C=O) and ether (C–O) groups (from 2.3% to 9.9% and from 5.8% to 6.8%, respectively) and the shift to a higher binding energy (288.37 and 286.5 eV, respectively) in the used sample, suggest the formation of reactive surface carbon species. More specifically the peak at 286.5 eV in the C1s spectra of the used sample has been associated with the formation of the CH_3O* feature (methoxy radical or activated methanol species) [103,104], which seems to be confirmed by the appearance of a XPS peak at about 531.2 eV in the O1s spectra of the used sample [105].

Ma et al. [105] studied the formation of intermediates on the Cu_2O/Cu (111) surface during CO_2 hydrogenation over a copper based catalyst. According to these studies, the C1s peak in the binding energy range of 286.1–286.5 eV can attributed to different species based on oxygenated hydrocarbons (HxCO) such as CO*, CH_3O*or *H_2CO on Cu-oxide and

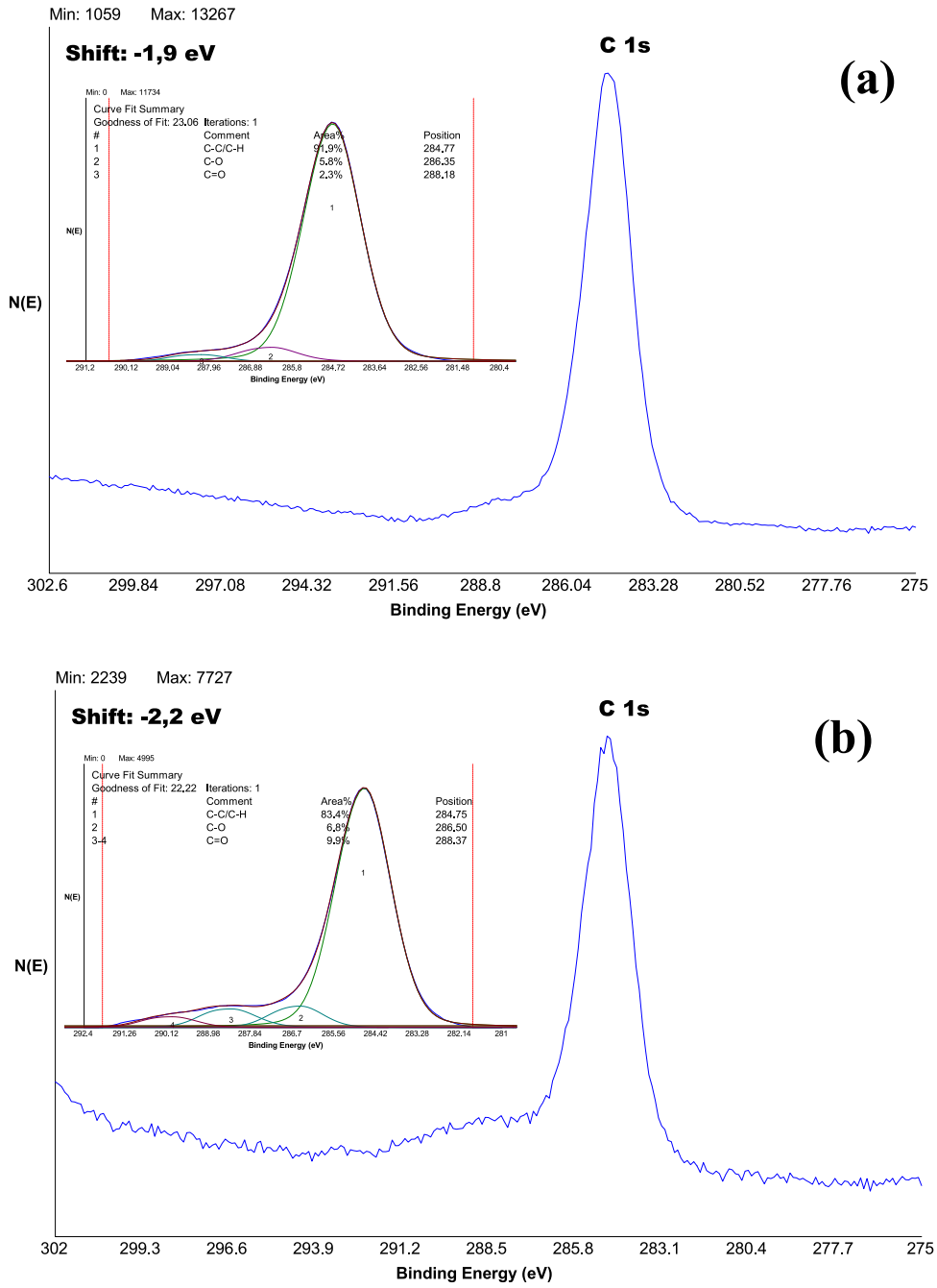

Fig. 7 – C 1s XPS spectra of the Cu cathode film: (a) as prepared and (b) after reduction and testing.

metallic Cu surfaces, with methoxy intermediate (CH_3O*) being the predominant at temperatures higher than 327 °C, which can be also the reason for the observed in-usual high value of selectivity to CH_4 at positive potentials, as it has been reported that the presence of adsorbed CH_3OH may block active sites for CO production via the RWGS reaction while forming adsorbed intermediates species (such as CH_3O*) which enhanced the methanation reaction [38]. The C1s peak in the binding energy range of 288–290 eV was ascribed instead to the presence of CO_2*/HCOO*, CO_3^{2-} or HxCO, with the latest oxygenated hydrocarbon (coke) based species, such as COH*, which is thought to be the reaction intermediate at negative potentials, being predominant at temperatures above 327 °C [105].

Fig. 8 shows the effect of applied potential on the rates of formation of CH_4 and CO on the Cu cathode film.

Normally, methanation reaction exhibits an electrophobic electrochemical behaviour, i.e. the rate of CH_4 formation diminishes with potential decrease, whereas Reverse Water Gas Shift (RWGS) reaction tend to be electrophilic, i.e. the rate of CO formation increases with decreasing applied potential over both proton (BZY) [47,54,58], and oxygen ion (YSZ) [50] conducting solid electrolytes. However, due to the co-ionic nature of the BZCY electrolyte, the electrochemical reactions

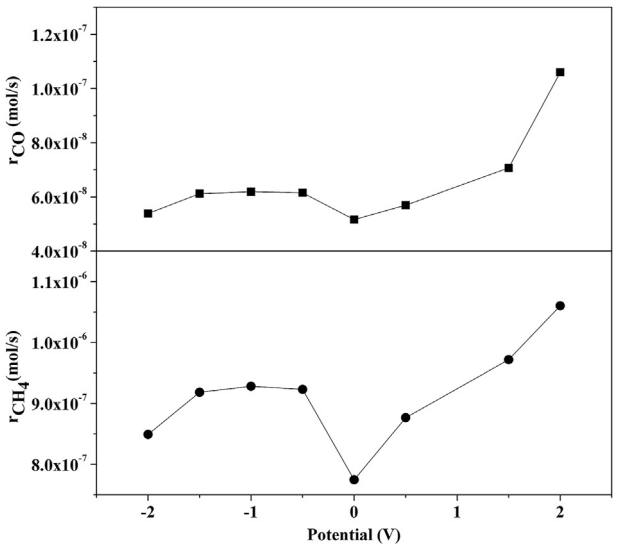

Fig. 8 – Influence of applied potential on the rates of (●) CH_4 and (■) CO formation over the Cu cathode film. (1 bar, 42 NL/h, $H_2/CO_2 = 4$, 450 °C).

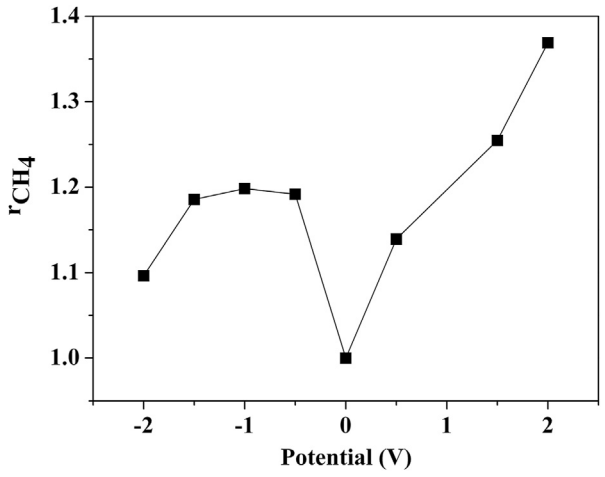

Fig. 9 – Influence of the applied potential on rate enhancement ratio (ρ) of CH_4. (1 bar, 42 NL/h, $H_2/CO_2 = 4$, 450 °C).

conducted in this work seem to present both behaviours, which vary upon polarization. The system seems to exhibit an "inverted volcano" electrochemical behaviour on CO_2 hydrogenation to both CH_4 and CO, showing a local minimum at around open circuit conditions (around 0V). Thus, it can be stated that both formation reactions show electrophobic behaviour at positive potentials (increase in catalytic rate at increasing positive potentials) and an electrophilic behaviour at negative ones (increase in catalytic rate at decreasing negative potentials). However, at highly negative potentials (<-1 V), the catalytic rate of CH_4 and CO formation diminishes on decreasing applied potential, supposedly due to the previously commented inhibiting effect of the excess of surface hydrogen coverage on the CO_2 hydrogenation reaction. Kalaitzidou et al. [48] carried out a comparative study of the electrochemical promotion of CO_2 hydrogenation on Ru using proton (BZY) and oxygen (YSZ) ion conducting solid electrolytes. They analysed also the effect of applied potential on CH_4 and CO selectivity and conversion rate. By comparison with the results presented in this work, it can be noted that the electrochemical behaviour for methanation reaction displayed using a co-ionic (H^+ and O^{2-}) ion conducting solid electrolyte (BZCY) (this work) almost resemble an intermediate situation between those reported using BZY and YSZ [48].

Fig. 9 shows the variation of the rate enhancement ratio of CH_4 (ρCH_4) with the applied potential.

It can be observed that negative potential application, i.e. H^+ supply to, and O^{2-} removal from the Cu catalyst surface, leads to rate enhancement ratios of about 1.1–1.2, whereas positive potential application, i.e. proton removal from, and migration of oxygen promoters to the Cu catalyst surface, leads to a slight more pronounced electropromotion obtaining higher ρ values of 1.2 or 1.4 at 1.5 and 2 V, respectively. Values of $\rho > 1$ is a distinctive attribute of electrochemical promotion vs. electrocatalysis [32]. In addition, the bigger the ρ value, the bigger the NEMCA effect.

The Cu catalyst exhibited an "inverted volcano type" electrochemical behaviour, i.e., CO_2 methanation rate enhancement ratio shows a minimum under open circuit conditions (at around 0 V) [32] (Fig. 9). This behaviour can be attributed to the increase of CO_2 (electron acceptor) and hydrogen (electron donor) chemisorptive strength and surface coverage under negative and positive polarization, correspondingly, as predicted by the rules governing electrochemical promotion [38,44]. The variance in the rate enhancement ratio of CH_4 in Fig. 9 upon positive and negative polarization can be ascribed to the different tendency to chemisorption of CO_2 and H_2 on Cu. H_2 is less easily adsorbed on Cu in comparison with CO_2 [106], therefore, the improvement of H_2 chemisorption by application of positive potentials is anticipated to have a more substantial impact on the CO_2 methanation rate. However, at highly negative potentials ($V < -1$ V), the CO_2 methanation rate enhancement ratio diminishes on decreasing applied potential, supposedly due to the previously commented inhibiting effect of the excess of surface hydrogen coverage on the CO_2 hydrogenation reaction.

Fig. 10 shows the variation of apparent faradaic efficiency ($|\Lambda|$) of CH_4 with applied potential, under the same conditions.

As can be observed in Fig. 10, $|\Lambda| > 1$ at all applied potentials apart from −2 V, the highest values of $|\Lambda|$ can be appreciated at −0.5 and 2 V and resulted to be 5.5 and 5.9, respectively. Values of $|\Lambda| > 1$ is a differentiating attribute of electrochemical promotion vs. electrocatalysis [32]. In addition, the bigger the $|\Lambda|$, the bigger the NEMCA effect.

Vayenas et al. [92] have reported to achieve NEMCA factor values of 74000 and rate enhancement ratios of 100. However, it must also be highlighted that their studies were conducted at very small-scale electrochemical cells with current values of 1 μA, which consequently leaded to faradaic rates in the order of 10^{-11} and 10^{-12} mol/s, and thus to very high Λ (according to (8)). Other hydrogenation studies similar to the one presented here, such as that of Kalaitzidou et al. [47], claim to achieve Λ_{CH4} values of above 500 and ρ_{CH4} of up to 4. Yet again, conditions applied in their work are far from realistic ones.

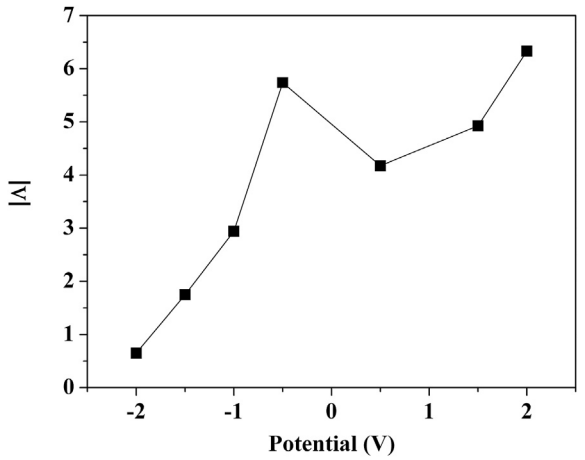

Fig. 10 – Influence of the applied potential on apparent faradaic efficiency or NEMCA factor (Λ) of CH_4. (1 bar, 42 NL/h, $H_2/CO_2 = 4$, 450 °C).

Experiments were carried on a lab-scale disk electrochemical cell using H_2 and CO_2 diluted in Helium and fed into the reactor at very small partial pressures (CO_2 at 0.25–2.3 kPa and H_2 at 1–15 kPa). In other words, considering they were conducted at atmospheric pressure (≈1 bar), flow rates represented between 0.25 and 2.3% for CO_2 and 1–15% for H_2 of the total gas injected into the reactor. Analogously to the studies conducted by Vayenas et al. [92], the utilization of such small reaction configurations allowed the induction of currents in the range of 400–800 μA and thus, higher values of Λ and ρ. On the contrary, a recent study by Chatzilias et al. [50] on CO_2 hydrogenation using high gas flow rates and a monolithic reaction configuration, reported values of Λ_{CH4} up to about 5 and of ρ_{CH4} up to around 1.4, more in line with those obtained in the present work.

Fig. 11 shows the influence of applied potential on the Faradaic or current efficiency (η_c), in parts per unit, and on the energy cost (C_E), in kWh per kg of methane.

The electrical energy required for producing methane can be assessed from the values of current efficiency (9) and energy cost (10) calculated for CH_4 formation. As can be derived from Fig. 11, the maximum value of Faradaic efficiency was obtained for −0.5 V and resulted to be 33.5, which corresponds to the minimum value of energy cost (0.002 kWh/kg). According to these results, −0.5 V is the optimal voltage potential for CH_4 formation from an efficiency and cost-reduction point of view.

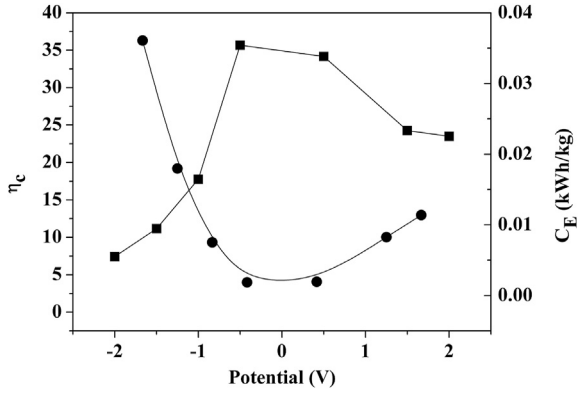

Fig. 11 – Influence of the applied potential on Faradaic efficiency (■) and energy cost (●). (1 bar, 42 NL/h, $H_2/CO_2 = 4$, 450 °C).

4. Conclusions

CO_2 methanation was investigated over a Cu cathode catalyst in a tubular co-ionic Solid Oxide Electrolyte Cell. In comparison to conventional fixed bed catalytic methanation reactors, the proposed reaction configuration potentially combines the advantages anticipated for the electrochemically assisted CO_2 methanation and for co-ionic (H^+/O^{2-} conducting) intermediate temperature electrolyte membrane reactors. The former would allow shifting the reaction equilibrium at atmospheric pressure, via electrochemical proton pumping to the catalyst, instead of using high pressures, in the range of 1–100 bar, typical for conventional reactors; increasing the reaction rate, by electrochemical O^{2-} removal from the catalyst, rendering higher conversion per pass and lower residence time, reactor size (CAPEX) and energy costs for preheating or compression (OPEX); enhancing the selectivity to CH_4, by electrochemically tuning H_2/CO_2 surface ratio, resulting in higher energy efficiency and lower purification costs (OPEX); increasing catalyst poison tolerance, by electrochemically retarding their chemisorption, and catalyst life time, by in-situ electrochemical tuning of catalyst activity/selectivity or regeneration, reducing the cost associated with catalyst regeneration or replacement (OPEX) and in-situ process control and monitoring (use as an electrochemical sensor), lowering CAPEX and OPEX associated with process instrumentation and control. Moreover, the double chamber reactor configuration (SOEC) would allow the integration of H_2O electrolysis or other hydrogen producing reaction (endothermic) and CO_2 methanation (exothermic) in the same system, enabling renewable energy storage in a more compact and smaller system, with adequate thermal control of the whole, resulting in energy savings and reduced CAPEX and OPEX against conventional fixed-bed reactors, where intermediate cooling steps or gas recycling are used for controlling methanation temperature.

The Cu electrocatalytic film (cathode), active for CO_2 methanation, was successfully coated by electroless on a commercial (CoorsTek Membrane Sciences) anode (Ni-BZCY)-supported solid electrolyte (BZCY) candle and afterwards characterized, both as prepared and after testing, by SEM-EDX, XRD and XPS. Characterization results revealed that electroless technique allowed the deposition of a thin Cu film (<2 μm), rendering a low electrical resistance and enhanced proton transfer to the cathode surface and reactant/product diffusion.

Electrochemically assisted CO_2 methanation was studied under atmospheric pressure, at intermediate temperatures (ranging between 325 °C and 550 °C), using relatively high gas flowrates (up to 42NL/h) and a realistic gas composition ($4H_2/CO_2$ binary mixture), representative of concentrated CO_2 capture exiting streams and renewable electrolytic hydrogen, and in an easy-scalable tubular cell configuration. CH_4 preferentially forms over CO under the utilized operating

conditions. CH_4 selectivity increases with temperature up to 97.3% at 400 °C. At higher temperatures, CH_4 and CO selectivity decreases and increases with temperature up to 79% and 21%, respectively. A temperature of 450 °C was finally selected to assure high values of co-ionic conductivity of BZCY and CH_4 yield. The control of CH_4 production can be carried out by modifying the applied potential, existing an optimal potential value, of about −0.5 V, which maximizes CH_4 selectivity (94.2%). In addition, under these conditions, high values of CO_2 conversion (32.5%) were obtained together with a maximum in Faradaic efficiency (33.5) and a minimum in energy cost (0.002 kWh/kg CH_4) and with a low selectivity to CO (5.8%), which results in greater production of CH_4 with a higher purity, which implies also a lower cost associated with the purification of the product.

Therefore, this study addresses some aspects, such as operation at high gas flow rates and, under atmospheric pressure and using representative gas compositions and easily scalable tubular cell configurations, based on a non-precious, widespread and cost-effective Cu cathode catalyst and commercially available solid electrolyte supports, and prepared by viable techniques, which may contribute to the development of effective cathode materials for CO_2 methanation in SOECs and to the optimization of cell operating conditions, such as temperature and applied potential, for increasing the energy efficiency and decreasing the costs of the process in order to fulfil the key challenges for advancing the process application. However, there are still research opportunities to improve the performance of the proposed co-ionic SOEC configuration towards CO_2 methanation, such as increasing the activity, selectivity and stability of the cathode electrocatalyst, by decreasing its particle size and increasing its dispersion or by addition of promoters or co-catalysts; reducing the ohmic losses by decreasing the thickness and increasing the electronic conductivity of the cathode electrode and the study of the long-term performance of the cathode catalyst under realistic conditions at a proper scale.

Declaration of competing interest

The authors declare that they have no known competing financial interests or personal relationships that could have appeared to influence the work reported in this paper.

Acknowledgements

The authors wish to thank CoorsTek Membrane Sciences for providing the anode supported solid oxide electrolyte tube.

REFERENCES

[1] Olah GA, Goeppert A, Prakash GKS. Chemical recycling of carbon dioxide to methanol and dimethyl ether: from greenhouse gas to renewable, environmentally carbon neutral fuels and synthetic hydrocarbons. J Org Chem 2009;74:487–98. https://doi.org/10.1021/jo801260f.

[2] Bossel U, Eliasson B, Taylor G. The future of the hydrogen economy: bright or bleak? Cogener Compet Power J 2003;18:29–70. https://doi.org/10.1080/15453660309509023.

[3] Linnér B-O, Wibeck V. Sustainability transformations: agents and drivers across societies. Cambridge: Cambridge University Press; 2019. https://doi.org/10.1017/9781108766975.

[4] Biswas S, Kulkarni AP, Giddey S, Bhattacharya S. A review on synthesis of methane as a pathway for renewable energy storage with a focus on solid oxide electrolytic cell-based processes. Front Energy Res 2020;8:570112. https://doi.org/10.3389/fenrg.2020.570112.

[5] Li W, Wang H, Shi Y, Cai N. Performance and methane production characteristics of H_2O–CO_2 co-electrolysis in solid oxide electrolysis cells. Int J Hydrogen Energy 2013;38:11104–9. https://doi.org/10.1016/j.ijhydene.2013.01.008.

[6] Jensen SH, Høgh JVT, Barfod R, Mogensen MB. High temperature electrolysis of steam and carbon dioxide. In: Petersen LS, Larsen H, editors. Energy technologies for post Kyoto targets in the medium term. Proceedings; 2003. p. 204–15. Denmark.

[7] Biswas S, Kulkarni AP, Fini D, Giddey S, Bhattacharya S. In situ synthesis of methane using Ag–GDC composite electrodes in a tubular solid oxide electrolytic cell: new insight into the role of oxide ion removal. Sustain Energy Fuels 2021;5:2055–64. https://doi.org/10.1039/D0SE01887B.

[8] Bierschenk DM, Wilson JR, Barnett SA. High efficiency electrical energy storage using a methane–oxygen solid oxide cell. Energy Environ Sci 2011;4:944–51. https://doi.org/10.1039/C0EE00457J.

[9] Xie K, Zhang Y, Meng G, Irvine JTS. Direct synthesis of methane from CO_2/H_2O in an oxygen-ion conducting solid oxide electrolyser. Energy Environ Sci 2011;4:2218–22. https://doi.org/10.1039/C1EE01035B.

[10] Chen L, Chen F, Xia C. Direct synthesis of methane from CO_2–H_2O co-electrolysis in tubular solid oxide electrolysis cells. Energy Environ Sci 2014;7:4018–22. https://doi.org/10.1039/C4EE02786H.

[11] Lei L, Liu T, Fang S, Lemmon JP, Chen F. The co-electrolysis of CO_2–H_2O to methane via a novel micro-tubular electrochemical reactor. J Mater Chem A 2017;5:2904–10. https://doi.org/10.1039/C6TA10252B.

[12] Biswas S, Kulkarni AP, Fini D, Singh Rathore S, Seeber A, Giddey S, et al. Catalyst-induced enhancement of direct methane synthesis in solid oxide electrolyser. Electrochim Acta 2021;391:138934. https://doi.org/10.1016/j.electacta.2021.138934.

[13] Luo Y, Li W, Shi Y, Cao T, Ye X, Wang S, et al. Experimental characterization and theoretical modeling of methane production by H_2O/CO_2 Co-electrolysis in a tubular solid oxide electrolysis cell. J Electrochem Soc 2015;162:F1129. https://doi.org/10.1149/2.0171510jes.

[14] Chen B, Xu H, Ni M. Modelling of SOEC-FT reactor: pressure effects on methanation process. Appl Energy 2017;185:814–24. https://doi.org/10.1016/j.apenergy.2016.10.095.

[15] Jensen SH, Langnickel H, Hintzen N, Chen M, Sun X, Hauch A, et al. Reversible operation of a pressurized solid oxide cell stack using carbonaceous gases. J Energy Storage 2019;22:106–15. https://doi.org/10.1016/j.est.2019.02.003.

[16] Lo Faro M, Oliveira da Silva W, Barrientos WV, Saglietti GGA, Zignani SC, Antonucci V, et al. Enhanced production of methane through the use of a catalytic Ni–Fe pre-layer in a solid oxide co-electrolyser. Int J Hydrogen Energy 2020;45:5134–42. https://doi.org/10.1016/j.ijhydene.2019.06.161.

[17] Baxter SJ, Rine M, Min B, Liu Y, Yao J. Near 100% CO_2 conversion and CH_4 selectivity in a solid oxide electrolysis cell with integrated catalyst operating at 450 °C. J CO2 Util 2022;59:101954. https://doi.org/10.1016/j.jcou.2022.101954.
[18] Pan Z, Duan C, Pritchard T, Thatte A, White E, Braun R, et al. High-yield electrochemical upgrading of CO_2 into CH_4 using large-area protonic ceramic electrolysis cells. Appl Catal, B 2022;307:121196. https://doi.org/10.1016/j.apcatb.2022.121196.
[19] Xie K, Zhang Y, Meng G, Irvine JTS. Electrochemical reduction of CO_2 in a proton conducting solid oxide electrolyser. J Mater Chem 2011;21:195–8. https://doi.org/10.1039/C0JM02205E.
[20] Li M, Hua B, Wang L-C, Sugar JD, Wu W, Ding Y, et al. Switching of metal–oxygen hybridization for selective CO_2 electrohydrogenation under mild temperature and pressure. Nat Catal 2021;4:274–83. https://doi.org/10.1038/s41929-021-00590-5.
[21] Duan C, Kee R, Zhu H, Sullivan N, Zhu L, Bian L, et al. Highly efficient reversible protonic ceramic electrochemical cells for power generation and fuel production. Nat Energy 2019;4:230–40. https://doi.org/10.1038/s41560-019-0333-2.
[22] Anastasijevic NA. NEMCA—from discovery to technology. Catal Today 2009;146:308–11. https://doi.org/10.1016/j.cattod.2009.02.020.
[23] Tsiplakides D, Balomenou S. Electrochemical promoted catalysis: towards practical utilization. Chem Ind Chem Eng Q 2008;14:97–105. https://doi.org/10.2298/CICEQ0802097T.
[24] Tsiplakides D, Balomenou S. Milestones and perspectives in electrochemically promoted catalysis. Catal Today 2009;146:312–8. https://doi.org/10.1016/j.cattod.2009.05.015.
[25] Caravaca A, González-Cobos J, Vernoux P. A discussion on the unique features of electrochemical promotion of catalysis (EPOC): are we in the right path towards commercial implementation? Catalysts 2020;10. https://doi.org/10.3390/catal10111276.
[26] Uhm S, Kim YD. Electrochemical conversion of carbon dioxide in a solid oxide electrolysis cell. Curr Appl Phys 2014;14:672–9. https://doi.org/10.1016/j.cap.2014.02.013.
[27] Ebbesen SD, Mogensen M. Electrolysis of carbon dioxide in solid oxide electrolysis cells. J Power Sources 2009;193:349–58. https://doi.org/10.1016/j.jpowsour.2009.02.093.
[28] Athanassiou C, Pekridis G, Kaklidis N, Kalimeri K, Vartzoka S, Marnellos G. Hydrogen production in solid electrolyte membrane reactors (SEMRs). Int J Hydrogen Energy 2007;32:38–54. https://doi.org/10.1016/j.ijhydene.2006.06.031.
[29] Kokkofitis C, Ouzounidou M, Skodra A, Stoukides M. High temperature proton conductors: applications in catalytic processes. Solid State Ionics 2007;178:507–13. https://doi.org/10.1016/j.ssi.2006.11.010.
[30] Xu D, Li K, Jia B, Sun W, Zhang W, Liu X, et al. Electrocatalytic CO_2 reduction towards industrial applications. Carbon Energy 2023;5:e230. https://doi.org/10.1002/cey2.230.
[31] Whipple DT, Kenis PJA. Prospects of CO_2 utilization via direct heterogeneous electrochemical reduction. J Phys Chem Lett 2010;1:3451–8. https://doi.org/10.1021/jz1012627.
[32] Vayenas CG, Bebelis S, Pliangos C, Brosda S, Tsiplakides D. Electrochemical activation of catalysis: promotion, electrochemical promotion, and metal-support interactions. New York: Kluwer Academic/Plenum Publishers; 2001. https://doi.org/10.1007/b115566.
[33] Sundmacher K, Rihko-Struckmann LK, Galvita V. Solid electrolyte membrane reactors: status and trends. Catal Today 2005;104:185–99. https://doi.org/10.1016/j.cattod.2005.03.074.
[34] Kyun Kim S, Kwon Y-i, Beom Kim Y, Jung J, Kang S, Hoon Joo J. Novel approach to integrate CO_2 utilization coupled with direct methane conversion to C2 products using solid oxide electrolysis cell. Chem Eng J 2022;444:136619. https://doi.org/10.1016/j.cej.2022.136619.
[35] Rönsch S, Schneider J, Matthischke S, Schlüter M, Götz M, Lefebvre J, et al. Review on methanation – from fundamentals to current projects. Fuel 2016;166:276–96. https://doi.org/10.1016/j.fuel.2015.10.111.
[36] Götz M, Lefebvre J, Mörs F, McDaniel Koch A, Graf F, Bajohr S, et al. Renewable Power-to-Gas: a technological and economic review. Renew Energy 2016;85:1371–90. https://doi.org/10.1016/j.renene.2015.07.066.
[37] Marnellos G, Stoukides M. Catalytic studies in electrochemical membrane reactors. Solid State Ionics 2004;175:597–603. https://doi.org/10.1016/j.ssi.2004.03.038.
[38] Papaioannou EI, Souentie S, Hammad A, Vayenas CG. Electrochemical promotion of the CO_2 hydrogenation reaction using thin Rh, Pt and Cu films in a monolithic reactor at atmospheric pressure. Catal Today 2009;146:336–44. https://doi.org/10.1016/j.cattod.2009.06.008.
[39] Pekridis G, Kalimeri K, Kaklidis N, Vakouftsi E, Iliopoulou EF, Athanasiou C, et al. Study of the reverse water gas shift (RWGS) reaction over Pt in a solid oxide fuel cell (SOFC) operating under open and closed-circuit conditions. Catal Today 2007;127:337–46. https://doi.org/10.1016/j.cattod.2007.05.026.
[40] Lymperi A, Chatzilias C, Xydas F, Martino E, Kyriakou G, Katsaounis A. Electrochemical promotion of CO_2 hydrogenation using a Pt/YSZ fuel cell type reactor. Preprints.org. 2023. https://doi.org/10.20944/preprints202304.0685.v1.
[41] Karagiannakis G, Zisekas S, Stoukides M. Hydrogenation of carbon dioxide in a proton conducting cell reactor. Ionics 2002;8:123–7. https://doi.org/10.1007/BF02377762.
[42] Bebelis S, Karasali H, Vayenas CG. Electrochemical promotion of the CO_2 hydrogenation on Pd/YSZ and Pd/β″-Al_2O_3 catalyst-electrodes. Solid State Ionics 2008;179:1391–5. https://doi.org/10.1016/j.ssi.2008.02.043.
[43] Bebelis S, Karasali H, Vayenas C. Electrochemical promotion of CO_2 hydrogenation on Rh/YSZ electrodes. J Appl Electrochem 2008;38:1127–33. https://doi.org/10.1007/s10800-008-9574-7.
[44] Theleritis D, Souentie S, Siokou A, Katsaounis A, Vayenas CG. Hydrogenation of CO_2 over Ru/YSZ electropromoted catalysts. ACS Catal 2012;2:770–80. https://doi.org/10.1021/cs300072a.
[45] Theleritis D, Makri M, Souentie S, Caravaca A, Katsaounis A, Vayenas CG. Comparative study of the electrochemical promotion of CO_2 hydrogenation over Ru-supported catalysts using electronegative and electropositive promoters. Chemelectrochem 2014;1:254–62. https://doi.org/10.1002/celc.201300185.
[46] Makri M, Katsaounis A, Vayenas CG. Electrochemical promotion of CO_2 hydrogenation on Ru catalyst–electrodes supported on a K–β″–Al_2O_3 solid electrolyte. Electrochim Acta 2015;179:556–64. https://doi.org/10.1016/j.electacta.2015.03.144.
[47] Kalaitzidou I, Katsaounis A, Norby T, Vayenas CG. Electrochemical promotion of the hydrogenation of CO_2 on Ru deposited on a BZY proton conductor. J Catal 2015;331:98–109. https://doi.org/10.1016/j.jcat.2015.08.023.
[48] Kalaitzidou I, Makri M, Theleritis D, Katsaounis A, Vayenas CG. Comparative study of the electrochemical promotion of CO_2 hydrogenation on Ru using Na^+, K^+, H^+ and O^{2-} conducting solid electrolytes. Surf Sci

2016;646:194–203. https://doi.org/10.1016/j.susc.2015.09.011.
[49] Makri M, Symillidis A, Grigoriou D, Katsaounis A, Vayenas CG. Electrochemical promotion of CO_2 reduction on a dispersed Ru/YSZ catalyst supported on YSZ solid electrolyte. Mater Today Proc 2018;5:27617–25. https://doi.org/10.1016/j.matpr.2018.09.082.
[50] Chatzilias C, Martino E, Katsaounis A, Vayenas CG. Electrochemical promotion of CO_2 hydrogenation in a monolithic electrochemically promoted reactor (MEPR). Appl Catal, B 2021;284:119695. https://doi.org/10.1016/j.apcatb.2020.119695.
[51] Chatzilias C, Martino E, Vayenas CG, Kyriakou G, Katsaounis A. A low temperature SOFC as a self-promoted reactor for CO_2 catalytic hydrogenation. Appl Catal, B 2022;317:121778. https://doi.org/10.1016/j.apcatb.2022.121778.
[52] Chatzilias C, Martino E, Tsatsos S, Kyriakou G, Katsaounis A, Vayenas CG. Kinetic study of CO_2 hydrogenation on Ru/YSZ catalyst using a monolithic electropromoted reactor (MEPR). Chem Eng J 2022;430:132967. https://doi.org/10.1016/j.cej.2021.132967.
[53] Panaritis C, Michel C, Couillard M, Baranova EA, Steinmann SN. Elucidating the role of electrochemical polarization on the selectivity of the CO_2 hydrogenation reaction over Ru. Electrochim Acta 2020;350:136405. https://doi.org/10.1016/j.electacta.2020.136405.
[54] Zagoraios D, Panaritis C, Krassakopoulou A, Baranova EA, Katsaounis A, Vayenas CG. Electrochemical promotion of Ru nanoparticles deposited on a proton conductor electrolyte during CO_2 hydrogenation. Appl Catal, B 2020;276:119148. https://doi.org/10.1016/j.apcatb.2020.119148.
[55] Jiménez V, Jiménez-Borja C, Sánchez P, Romero A, Papaioannou EI, Theleritis D, et al. Electrochemical promotion of the CO_2 hydrogenation reaction on composite Ni or Ru impregnated carbon nanofiber catalyst-electrodes deposited on YSZ. Appl Catal, B 2011;107:210–20. https://doi.org/10.1016/j.apcatb.2011.07.016.
[56] Gutiérrez-Guerra N, González-Cobos J, Serrano-Ruiz JC, Valverde JL, de Lucas-Consuegra A. Electrochemical activation of Ni catalysts with potassium ionic conductors for CO_2 hydrogenation. Top Catal 2015;58:1256–69. https://doi.org/10.1007/s11244-015-0488-4.
[57] Zagoraios D, Kokkinou N, Kyriakou G, Katsaounis A. Electrochemical control of the RWGS reaction over Ni nanoparticles deposited on yttria stabilized zirconia. Catal Sci Technol 2022;12:1869–79. https://doi.org/10.1039/D1CY02140K.
[58] Kotsiras A, Kalaitzidou I, Grigoriou D, Symillidis A, Makri M, Katsaounis A, et al. Electrochemical promotion of nanodispersed Ru-Co catalysts for the hydrogenation of CO_2. Appl Catal, B 2018;232:60–8. https://doi.org/10.1016/j.apcatb.2018.03.031.
[59] Panaritis C, Zgheib J, Ebrahim SAH, Couillard M, Baranova EA. Electrochemical in-situ activation of Fe-oxide nanowires for the reverse water gas shift reaction. Appl Catal, B 2020;269:118826. https://doi.org/10.1016/j.apcatb.2020.118826.
[60] Panaritis C, Zgheib J, Couillard M, Baranova EA. The role of Ru clusters in Fe carbide suppression for the reverse water gas shift reaction over electropromoted Ru/FeOx catalysts. Electrochem Commun 2020;119:106824. https://doi.org/10.1016/j.elecom.2020.106824.
[61] Díez-Ramírez J, Sánchez P, Valverde JL, Dorado F. Electrochemical promotion and characterization of PdZn alloy catalysts with K and Na ionic conductors for pure gaseous CO_2 hydrogenation. J CO2 Util 2016;16:375–83. https://doi.org/10.1016/j.jcou.2016.09.007.
[62] Karagiannakis G, Zisekas S, Stoukides M. Hydrogenation of carbon dioxide on copper in a H^+ conducting membrane-reactor. Solid State Ionics 2003;162–163:313–8. https://doi.org/10.1016/S0167-2738(03)00227-3.
[63] Wang J, Couillard M, Baranova EA. Electrochemical promotion of copper nanoparticles for the reverse water gas shift reaction. Catal Sci Technol 2022;12:1562–73. https://doi.org/10.1039/D1CY02315B.
[64] Wang J, Couillard M, Baranova EA. Insight into electrochemical promotion of Cu/Co_3O_4 catalysts for the reverse water gas shift reaction. ChemCatChem 2023;15:e202201514. https://doi.org/10.1002/cctc.202201514.
[65] Ruiz E, Cillero D, Martínez PJ, Morales Á, Vicente GS, de Diego G, et al. Bench scale study of electrochemically promoted catalytic CO_2 hydrogenation to renewable fuels. Catal Today 2013;210:55–66. https://doi.org/10.1016/j.cattod.2012.10.025.
[66] Ruiz E, Cillero D, Martínez PJ, Morales Á, Vicente GS, de Diego G, et al. Electrochemical synthesis of fuels by CO_2 hydrogenation on Cu in a potassium ion conducting membrane reactor at bench scale. Catal Today 2014;236:108–20. https://doi.org/10.1016/j.cattod.2014.01.016.
[67] Ruiz E, Cillero D, Martínez PJ, Morales Á, Vicente GS, de Diego G, et al. Bench-scale study of electrochemically assisted catalytic CO_2 hydrogenation to hydrocarbon fuels on Pt, Ni and Pd films deposited on YSZ. J CO_2 Util 2014;8:1–20. https://doi.org/10.1016/j.jcou.2014.09.001.
[68] Ruiz E, Martínez PJ, Morales Á, San Vicente G, de Diego G, Sánchez JM. Electrochemically assisted synthesis of fuels by CO_2 hydrogenation over Fe in a bench scale solid electrolyte membrane reactor. Catal Today 2016;268:46–59. https://doi.org/10.1016/j.cattod.2016.02.025.
[69] Wei W, Jinlong G. Methanation of carbon dioxide: an overview. Front Chem Sci Eng 2011;5:2–10. https://doi.org/10.1007/s11705-010-0528-3.
[70] Peterson AA, Abild-Pedersen F, Studt F, Rossmeisl J, Nørskov JK. How copper catalyzes the electroreduction of carbon dioxide into hydrocarbon fuels. Energy Environ Sci 2010;3:1311–5. https://doi.org/10.1039/C0EE00071J.
[71] Nie X, Luo W, Janik MJ, Asthagiri A. Reaction mechanisms of CO_2 electrochemical reduction on Cu(111) determined with density functional theory. J Catal 2014;312:108–22. https://doi.org/10.1016/j.jcat.2014.01.013.
[72] Wu B, Chen J, Qian L. Recent advances in heterogeneous electroreduction of CO_2 on copper-based catalysts. Catalysts 2022;12. https://doi.org/10.3390/catal12080860.
[73] Kyriakou V, Garagounis I, Vourros A, Vasileiou E, Manerbino A, Coors WG, et al. Methane steam reforming at low temperatures in a $BaZr_{0.7}Ce_{0.2}Y_{0.1}O_{2.9}$ proton conducting membrane reactor. Appl Catal, B 2016;186:1–9. https://doi.org/10.1016/j.apcatb.2015.12.039.
[74] Favaro M, Xiao H, Cheng T, Goddard W, Yano J, Crumlin E. Subsurface oxide plays a critical role in CO_2 activation by Cu(111) surfaces to form chemisorbed CO_2, the first step in reduction of CO_2. Proc Natl Acad Sci USA 2017;114:201701405. https://doi.org/10.1073/pnas.1701405114.
[75] Harvey S, Ricote S, Diercks D, Jiang C-S, Patki N, Manerbino A, et al. Evolution of copper electrodes fabricated by electroless plating on $BaZr_{0.7}Ce_{0.2}Y_{0.1}O_{3-\delta}$ proton-conducting ceramic membrane: from deposition to testing in methane. Ceramics 2018;1:261–73. https://doi.org/10.3390/ceramics1020021.

[76] Hernández Morejudo S, Zanon R, Escolástico S, Yuste-Tirados I, Fjeld H, Vestre P, et al. Direct conversion of methane to aromatics in a catalytic co-ionic membrane reactor. Science 2016;353:563–6. https://doi.org/10.1126/science.aag0274.
[77] Patki NS, Way JD, Ricote S. High performance fuel electrodes fabricated by electroless plating of copper on $BaZr_{0.8}Ce_{0.1}Y_{0.1}O_{3-\delta}$ proton-conducting ceramic. J Power Sources 2017;365:399–407. https://doi.org/10.1016/j.jpowsour.2017.08.098.
[78] Patki NS, Ricote S, Way JD. Fabrication of reducing atmosphere electrodes (fuel electrodes) by electroless plating of copper on $BaZr_{0.9-x}Ce_xY_{0.1}O_{3-\delta}$ – a proton-conducting ceramic. Int J Hydrogen Energy 2017;42:16911–9. https://doi.org/10.1016/j.ijhydene.2017.06.029.
[79] Davis JR. Copper and copper alloys. Ohio: ASM international; 2001.
[80] Inoue F, Philipsen H, Radisic A, Armini S, Civale Y, Leunissen P, et al. Electroless Cu deposition on atomic layer deposited Ru as novel seed formation process in through-Si vias. Electrochim Acta 2013;100:203–11. https://doi.org/10.1016/j.electacta.2013.03.106.
[81] Komatsu S, Tanaka M, Okumura A, Kungi A. Preparation of cu-solid polymer electrolyte composite electrodes and application to gas-phase electrochemical reduction of CO_2. Electrochim Acta 1995;40:745–53. https://doi.org/10.1016/0013-4686(94)00325-U.
[82] Schaal MT, Metcalf AY, Montoya JH, Wilkinson JP, Stork CC, Williams CT, et al. Hydrogenation of 3,4-epoxy-1-butene over Cu–Pd/SiO_2 catalysts prepared by electroless deposition. Catal Today 2007;123:142–50. https://doi.org/10.1016/j.cattod.2007.01.015.
[83] Córdoba J, Odén M. Growth and characterization of electroless deposited Cu films on carbon nanofibers. Surf Coat Technol 2009;203:3459–64. https://doi.org/10.1016/j.surfcoat.2009.05.007.
[84] Morales A. EU EP 1 321 539 A2.
[85] Dandekar A, Vannice M. Determination of the dispersion and surface oxidation states of supported Cu catalysts. J Catal 1998;178:621–39. https://doi.org/10.1006/jcat.1998.2190.
[86] Chen C-S, You J-H, Lin J-H, Chen Y-Y. Effect of highly dispersed active sites of Cu/TiO_2 catalyst on CO oxidation. Catal Commun 2008;9:2381–5. https://doi.org/10.1016/j.catcom.2008.06.003.
[87] Yao X, Yu Q, Ji Z, Lv Y, Cao Y, Tang C, et al. A comparative study of different doped metal cations on the reduction, adsorption and activity of CuO/$Ce_{0.67}M_{0.33}O_2$ (M= Zr^{4+}, Sn^{4+}, Ti^{4+}) catalysts for NO+ CO reaction. Appl Catal, B 2013;130:293–304. https://doi.org/10.1016/j.apcatb.2012.11.020.
[88] Bergeret G, Gallezot P. Particle size and dispersion measurements. In: Handbook of heretogeneous Catalysis. Wiley-VCH; 2008. p. 738–65. https://doi.org/10.1002/9783527610044.hetcat0038.
[89] Guizard C, Princivalle A. Preparation and characterization of catalyst thin films. Catal Today 2009;146:367–77. https://doi.org/10.1016/j.cattod.2009.05.012.
[90] Choi S, Sang B-I, Hong J, Yoon KJ, Son J-W, Lee J-H, et al. Catalytic behavior of metal catalysts in high-temperature RWGS reaction: in-situ FT-IR experiments and first-principles calculations. Sci Rep 2017;7:41207. https://doi.org/10.1038/srep41207.
[91] Bausá N, Escolástico S, Serra JM. Direct CO_2 conversion to syngas in a $BaCe_{0.2}Zr_{0.7}Y_{0.1}O_{3-\delta}$-based proton-conducting electrolysis cell. J CO2 Util 2019;34:231–8. https://doi.org/10.1016/j.jcou.2019.05.037.
[92] Vayenas C, Ladas S, Bebelis S, Yentekakis I, Neophytides S, Yi J, et al. Electrochemical promotion in catalysis: non-faradaic electrochemical modification of catalytic activity. Electrochim Acta 1994;39:1849–55. https://doi.org/10.1016/0013-4686(94)85174-3.
[93] Freund H-J, Roberts MW. Surface chemistry of carbon dioxide. Surf Sci Rep 1996;25:225–73. https://doi.org/10.1016/S0167-5729(96)00007-6.
[94] Onsgaard J, Thomsen L, Hoffmann SV, Godowski PJ. Surface reactions between CO_2 and H over K-modified Cu (0 0 1). Vacuum 2006;81:25–31. https://doi.org/10.1016/j.vacuum.2006.02.005.
[95] Yin S, Ge Q. Selective CO_2 hydrogenation on the γ-Al_2O_3 supported bimetallic Co–Cu catalyst. Catal Today 2012;194:30–7. https://doi.org/10.1016/j.cattod.2012.01.011.
[96] Brisard G, Camargo APM, Nart FC, Iwasita T. On-line mass spectrometry investigation of the reduction of carbon dioxide in acidic media on polycrystalline Pt. Electrochem Commun 2001;3:603–7. https://doi.org/10.1016/S1388-2481(01)00223-5.
[97] Rendon-Calle A, Low QH, Hong SHL, Builes S, Yeo BS, Calle-Vallejo F. How symmetry factors cause potential-and facet-dependent pathway shifts during CO_2 reduction to CH_4 on Cu electrodes. Appl Catal, B 2021;285:119776. https://doi.org/10.1016/j.apcatb.2020.119776.
[98] Etim UJ, Semiat R, Zhong Z. CO_2 valorization reactions over Cu-based catalysts: characterization and the nature of active sites. Am J Chem Eng 2021;9:53–78. https://doi.org/10.11648/j.ajche.20210903.12.
[99] Hahn C, Hatsukade T, Kim Y-G, Vailionis A, Baricuatro JH, Higgins DC, et al. Engineering Cu surfaces for the electrocatalytic conversion of CO_2: controlling selectivity toward oxygenates and hydrocarbons. Proc Natl Acad Sci USA 2017;114:5918–23. https://doi.org/10.1073/pnas.1618935114.
[100] Ahmad T, Liu S, Sajid M, Li K, Ali M, Liu L, et al. Electrochemical CO_2 reduction to C_2^+ products using Cu-based electrocatalysts: a review. Nano Res Energy 2022;1:e9120021. https://doi.org/10.26599/NRE.2022.9120021.
[101] Shu Y, Ichikawa M. Catalytic dehydrocondensation of methane towards benzene and naphthalene on transition metal supported zeolite catalysts: templating role of zeolite micropores and characterization of active metallic sites. Catal Today 2001;71:55–67. https://doi.org/10.1016/S0920-5861(01)00440-0.
[102] Weckhuysen BM, Rosynek MP, Lunsford JH. Characterization of surface carbon formed during the conversion of methane to benzene over Mo/H-ZSM-5 catalysts. Catal Lett 1998;52:31–6. https://doi.org/10.1023/A:1019094630691.
[103] Clark DT, Thomas HR. Applications of ESCA to polymer chemistry. XVII. Systematic investigation of the core levels of simple homopolymers. J Polym Sci Polym Chem Ed 1978;16:791–820. https://doi.org/10.1002/pol.1978.170160407.
[104] Clark D, Cromarty B, Dilks A. A theoretical investigation of molecular core binding and relaxation energies in a series of oxygen-containing organic molecules of interest in the study of surface oxidation of polymers. J Polym Sci Polym Chem Ed 1978;16:3173–84. https://doi.org/10.1002/pol.1978.170161212.
[105] Ma Y, Wang J, Goodman KR, Head AR, Tong X, Stacchiola DJ, et al. Reactivity of a zirconia–copper inverse catalyst for CO_2 hydrogenation. J Phys Chem C 2020;124:22158–72. https://doi.org/10.1021/acs.jpcc.0c06624.
[106] Kuze H, Okude Si. Adsorption of CO_2 and H_2 on Cu and Zn micro-cluster surfaces studied by quantum chemistry and theory of absolute reaction rates. Open J Phys Chem 2011;1:109. https://doi.org/10.4236/ojpc.2011.13015.